Radiative corrections for $(e,e'p)$ reactions at GeV energies

R. Ent,[1,2] B. W. Filippone,[3] N. C. R. Makins,[1,*] R. G. Milner,[1] T. G. O'Neill,[3,†] and D. A. Wasson[4,‡]
[1]*Laboratory for Nuclear Science, Massachusetts Institute of Technology, Cambridge, Massachusetts 02139*
[2]*Thomas Jefferson National Accelerator Facility, Newport News, Virginia 23606*
[3]*W. K. Kellogg Radiation Laboratory, California Institute of Technology, Pasadena, California 94305*
[4]*Center for Theoretical Physics, Massachusetts Institute of Technology, Cambridge, Massachusetts 02139*
(Received 24 July 2000; published 12 October 2001)

A general framework for applying radiative corrections to $(e,e'p)$ coincidence reactions at GeV energies is presented, with special emphasis to higher-order bremsstrahlung effects, radiation from the scattered hadron, and the validity of peaking approximations. The sensitivity to the assumptions made in practically applying radiative corrections to $(e,e'p)$ data is extensively discussed. The general framework is tested against experimental data of the ^{1}H$(e,e'p)$ reaction at momentum transfer values larger than 1.0 $(\mathrm{GeV}/c)^2$, where radiative processes become a dominant source of uncertainty. The formulas presented here can easily be modified for any other electron-induced coincidence reaction.

DOI: 10.1103/PhysRevC.64.054610 PACS number(s): 25.30.Fj, 13.40.Ks, 13.60.−r, 24.10.Lx

I. INTRODUCTION

Coincidence $(e,e'p)$ reactions off nuclei can allow detailed studies of the nuclear wave function as well as quasielastic reaction dynamics. The attractiveness of electron scattering is that the photon couples weakly to the electron and proton, simplifying the extraction of information from experimental data. Unfortunately, photons are also massless and can be copiously produced in such experiments. Real photons are emitted (bremsstrahlung) when the charged particles involved in the reaction are accelerated by the fields of either the nucleus involved in the primary hard scattering (''internal radiation''), or by the other nuclei encountered by the incoming/outgoing particles as they travel through intervening material (''external radiation''). The emission of real photons causes a discrepancy between the detected particles' momenta and their actual momenta at the scattering vertex, and so causes distortions in the extracted experimental spectra. Conversely, amplitudes involving the emission of additional virtual photons affect only the magnitude of the measured cross section.

The topic of radiative corrections is an old one, dating back to Bethe and Heitler, who first calculated the bremsstrahlung spectrum of an electron scattering in a coulomb potential [1], and Schwinger, who first calculated the full first order radiative correction to this same problem [2]. For soft-photon emission, lowest order perturbation theory is inadequate. Yennie, Frautschi, and Suura generalized this result to higher orders, showing how to deal with soft-photon emission [3]. Tsai [4] and Meister and Yennie [5] derived explicit formulas for radiatively correcting inclusive elastic scattering of electrons off protons, where only the electron is detected. Finally, a review article by Mo and Tsai [6] summarized the approaches and approximations that could be used to radiatively correct data in different situations and discussed the advantages of the Tsai over the Meister and Yennie results. More recently, de Calan, Navelet, and Picard [7] derived a third set of formulas that disagree with the results of Tsai [4]. The current paper considers radiative corrections for coincidence $(e,e'p)$ reactions. Its goal is to emphasize the assumptions and ambiguities involved in radiative correction formulas, in particular the differences between Refs. [7,6], and to produce formulas applicable to coincidence reactions.

The primary cross sections of interest are the cross section for an electron to scatter off a proton into a solid angle $d\Omega_e$ and produce photons with total momentum in the range $d^3\omega$,

$$\frac{d\sigma}{d\Omega_e d^3\omega} \tag{1}$$

and the cross section for an electron to scatter off a proton into a solid angle $d\Omega_e$ without emitting photons whose total energy is greater than ΔE_m,

$$\frac{d\sigma}{d\Omega_e}(\omega < \Delta E_m). \tag{2}$$

The former cross section is necessary in order to propagate the radiative tail through missing energy and momentum space, while the later can be used if one only wants to measure the missing energy distribution with the missing momentum integrated out (four-momentum conservation can be used to determine the missing energy and momentum not accounted for in the detected particles—see Sec. II).

Within QED it is straightforward to calculate these cross sections to low orders in the fine structure constant α. However, electron-proton scattering also contains the strong interaction, which does not factor from the QED corrections. If we were interested in radiatively correcting electron-muon scattering this problem would not be severe. Both the first order elastic and bremsstrahlung cross sections would be un-

*Present address: Department of Physics, University of Illinois, Urbana, IL 61801.
†Present address: Sun Microsystems, Inc., Palo Alto, CA 94303.
‡Present address: Arete, Marina del Rey, CA 90292.

ambiguously determined, and only the vacuum polarization correction to the second order elastic cross section would have some uncertainties.

In the case of electron-proton scattering, the situation is more difficult. Neither the first order elastic or bremsstrahlung cross sections are calculable exactly due to the extended structure of the proton. For example, consider the expansion of Eq. (2) to first order in α, which can be parametrized as

$$\frac{d\sigma}{d\Omega_e}(\omega<\Delta E_m)=\left.\frac{d\sigma^{(1)}}{d\Omega_e}\right|_{ep}(1-\alpha[\delta_1(\Delta E_m)+\delta_2]), \quad (3)$$

where

$$\left.\frac{d\sigma^{(1)}}{d\Omega_e}\right|_{ep}$$

is the one-photon exchange (Born) electron-proton cross section and the order α radiative correction has been divided into two terms; the first due to bremsstrahlung of real photons (δ_1) and the second term caused by virtual particle corrections to the elastic cross section (δ_2). The choice of kinematics for the quasifree electron-proton scattering case is discussed in Sec. II. The first correction, $\delta_1(\Delta E_m)$, which determines the shape of the Bremsstrahlung spectra is fairly well-determined and will be discussed in Sec. III A. The second correction, δ_2 is not well determined and different formulas for radiative corrections to electron-proton scattering typically differ in their expressions for δ_2.

Fortunately, the choice of δ_2 is not too important, as long as it is done *consistently*. Radiative correction formulas, such as Eq. (3), are generally applied to electron-proton scattering data in order to determine $d\sigma^{(1)}/d\Omega_e$. Different choices of δ_2 change the extracted values of $d\sigma^{(1)}/d\Omega_e$. If one then uses these extracted cross sections in analyzing an $(e,e'p)$ reaction, as long as one uses the same δ_2 as was used in extracting $\sigma^{(1)}$, one will reproduce the correct cross section. These points will be discussed in Sec. III B.

The correct calculation of δ_1, on the other hand, is very important. The lowest order calculations work well for large photon energies but break down for small photon energies, where multiple-photon generation dominates. In this regime, the soft-photon bremsstrahlung diagrams need to be summed to all orders, which turns out to be equivalent to exponentiation. Recently, the necessity of including multiphoton emission was shown in a practical example for the ^{3}He$(e,e'p)$ reaction [8]. In contrast, this work provides a more rigorous framework on applying radiative corrections to coincidence $(e,e'p)$ reactions, evaluating the effect of the various contributions and assumptions in the many-GeV region. We further deal with the effects of multiphoton emission in Sec. III C.

In general, these multiphoton emission cross sections are too complicated to simply remove the effect of bremsstrahlung from experimental data. At high energies, the individual photons are largely emitted in the direction of the incoming or outgoing fermions. This allows the introduction of a peaking approximation that greatly simplifies the calculation of the angular distribution of the emitted photon radiation. This approximation is discussed in Sec. IV A. We discuss in Sec. IV B the spectrum for the emission of ''external'' radiation, which has essentially been discussed before by Tsai [9] and Friedrich [10]. We also discuss in this section the generalized peaking approximation, which adds the effects of ''internal'' and ''external'' radiation in a consistent manner in the peaking approximations applied.

Section V discusses the Monte Carlo simulation methods used to enable a comparison of the radiative corrections framework discussed with experimental (e,e') and $(e,e'p)$ data. In Sec. V A we describe the general Monte Carlo simulation method used, and how the radiative correction procedures were applied to this simulation. In Sec. V B comparisons of the described Monte Carlo simulation with experimental data from the Stanford Linear Accelerator Center (SLAC) experiment NE18 are shown [11]. Sec. V C discusses a ''modified'' equivalent radiator method, a straightforward Monte Carlo simulation method which for most $(e,e'p)$ experiments will be satisfactory to apply radiative corrections. Again comparisons of this Monte Carlo method with experimental data from the NE18 experiment are presented. Finally, Section VI provides a summary of the work presented.

II. KINEMATICS

This section considers the kinematics of the process

$$eA\rightarrow e'\gamma p(A-1)^*,$$

where the residual $(A-1)^*$ is an unmeasured state of $(A-1)$ nucleons plus any other particles produced in the reaction. Denote the initial and final four-momenta of the electron $k=(\epsilon,\mathbf{k})$ and $k'=(\epsilon',\mathbf{k}')$ respectively, the final four-momenta of the proton $p'=(p'^0,\mathbf{p}')$, the four-momentum $q=k-k'=(\nu,\mathbf{q})$ transferred from the electron, and the four-momenta of the bremsstrahlung photon $\omega=(\omega^0,\boldsymbol{\omega})$ where $\omega^0=|\boldsymbol{\omega}|$. The electron mass will be denoted m and the proton mass denoted M. For the discussion of kinematics in this section, the electron mass will be taken as negligible.

The real photon ω appears in the energy-momentum conservation relation as an additional four-momentum in the final state:

$$k+p_A=k'+p'+\omega+p^*_{(A-1)}. \quad (4)$$

All of these variables are four-momenta, representing respectively the initial electron, the initial target nucleus, the scattered electron, the knockout proton, the emitted photon, and the recoiling $(A-1)$ system (possibly in an excited state, as indicated by the asterisk). If one now denotes the values one *measures* for the missing momentum and energy by $\tilde{\mathbf{p}}_\mathbf{m}$ and $\tilde{E}_m$, and their vertex values *in the absence of radiation* by $\mathbf{p_m}$ and E_m, one obtains

$$\mathbf{p_m}=\mathbf{p}'+\boldsymbol{\omega}-\mathbf{q}=\tilde{\mathbf{p}}_\mathbf{m}+\boldsymbol{\omega},$$

$$E_m+T_{rec}=\epsilon-\epsilon'-(p'^0-M)-\omega^0=\tilde{E}_m+\tilde{T}_{rec}-\omega^0, \quad (5)$$

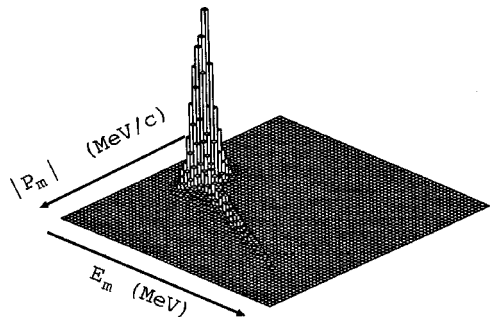

FIG. 1. Distribution of counts in E_m and $|p_m|$ for $(e,e'p)$ from hydrogen at $Q^2=1$ $(\mathrm{GeV}/c)^2$, demonstrating the existence of ''tails'' due to bremsstrahlung radiation. The E_m axis runs in the bottom-right direction, from -25 to 125 MeV in bins of 2.5 MeV; the $|p_m|$ axis runs towards bottom-left, from -160 to 160 MeV/c in bins of 5 MeV/c.

and so

$$\tilde{\mathbf{p}}_\mathbf{m}=\mathbf{p}_\mathbf{m}-\boldsymbol{\omega},$$

$$\tilde{E}_m=E_m+T_{rec}-\tilde{T}_{rec}+\omega^0\cong E_m+\omega^0. \tag{6}$$

Note that the measured value of the recoil kinetic energy, $\tilde{T}_{rec}$, depends on the measured missing momentum and so is also distorted by bremsstrahlung photons. However, the contribution of T_{rec} to the missing energy is, in general, small (and nonexistent in the case of elastic ep scattering). The approximation $\tilde{T}_{rec}\simeq T_{rec}$ is not used in the calculations described herein, but merely serves to illustrate the overall effect of radiation on a measured (E_m,p_m) distribution: the real photons produce long ''tails'' which, at very high photon energy $(\omega^0\gg E_m,p_m)$, are described by the relation $\tilde{E}_m\cong\tilde{p}_m\cong\omega^0$. Elastic ep scattering provides a clear demonstration of these tails, since in the absence of radiation, all strength is localized at $E_m=p_m=0$ (see Fig. 1). It is seen that the radiated events are distributed along the line with $E_m=|\vec{p}_m|$ as required for real photons.

The coincidence variables E_m and p_m thus provide a natural basis in which to evaluate radiative effects. By contrast, radiative corrections have generally been calculated in the framework of inclusive (e,e') experiments—in terms of their effect on the measured energy transfer ν $(=\epsilon-\epsilon')$. If we denote, similarly as above, $\tilde{\nu}$ $(\tilde{\mathbf{q}})$ as the measured energy (momentum) transfer, one obtains

$$\tilde{\mathbf{q}}=\mathbf{q}-\boldsymbol{\omega},$$

$$\tilde{\nu}=\nu+\omega^0. \tag{7}$$

The effect of radiation on these quantities depends on the direction of the emitted photon: Consider elastic scattering, with Born-level differential cross section $d\sigma^{(1)}/d\Omega_{e'}$. The reaction amplitude is fixed by the direction of the scattered electron (and, of course, the incident electron energy). If we treat this direction $\hat{k}'$ as fixed, the radiation of a photon parallel to $\hat{k}'$ simply decreases the energy ϵ' by the photon energy ω^0. If, however, the photon direction is parallel to the incoming electron, ϵ' is affected by an amount that depends on the electron scattering angle. (Note that the scattered proton vector is also affected.) Thus, when one comes to evaluate the total probability of emitting radiation that affects ν by less than some cutoff energy ΔE_m, one has to perform integrals over photon energy and direction with interdependent integration limits. In the case of coincidence scattering, independent integrals can be performed as the measurement of both scattered particles enables one to select a more ''natural'' choice of variables—E_m and p_m. In the elastic scattering example of above, if the missing energy is measured to an accuracy ΔE_m, one is guaranteed that all measured events correspond to emitted photons with less than ΔE_m, regardless of the photon direction, or, equivalently, the ratio of ϵ/ϵ'.

TABLE I. Kinematics settings used.

Q^2 $(\mathrm{GeV}/c)^2$	ϵ (GeV)	ϵ' (GeV)	θ_e (deg)
1	2.01	1.41	37.3
3	3.19	1.47	49.0
5	4.21	1.47	54.2
7	5.12	1.47	57.0
6	12.1	8.9	14.0
9	15.4	10.6	14.0
12	18.3	11.9	14.0
15	21.0	13.0	14.0

The formalism described in this section is based on the work of Mo and Tsai [4,6] which has provided the standard radiative corrections prescription for three decades of inclusive electron scattering experiments. The basic formulas of Mo and Tsai have been reevaluated in a coincidence framework: one can no longer integrate over all final states of the scattered proton as in (e,e') measurements, but must calculate the radiative effect on both the scattered electron and proton. The resulting distributions are then included in the event generation of a Monte Carlo simulation and folded with the experimental detection range in $\mathbf{k}'$ and $\mathbf{p}'$ as described earlier. Throughout this work we will use for the numerical examples the kinematics given in Table I and denote the specific kinematics with its momentum transfer squared value Q^2. Specifically, some of the kinematics given in the table are consistent with the kinematics of the NE18 experiment at SLAC [11].

III. INTERNAL BREMSSTRAHLUNG

A. First order internal bremsstrahlung

The probability for radiating a single bremsstrahlung photon is represented by the four Feynman diagrams of Fig. 2. Since each of these diagrams involves the same final state, the amplitudes must be summed coherently:

$$\frac{d\sigma}{d^3k'd^3\omega}\sim|\mathcal{M}_{\mathrm{ei}}+\mathcal{M}_{\mathrm{ef}}+\mathcal{M}_{\mathrm{pi}}+\mathcal{M}_{\mathrm{pf}}|^2. \tag{8}$$

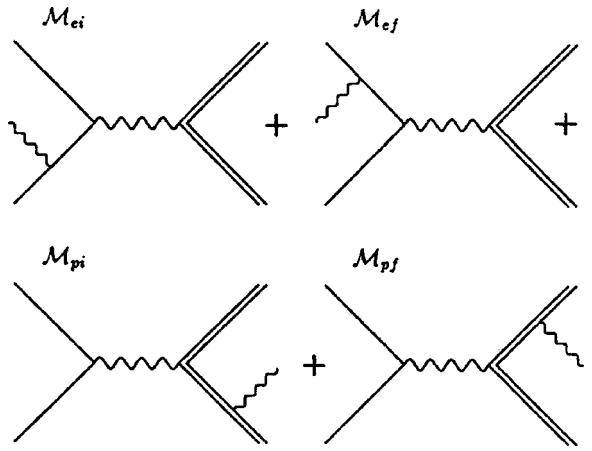

FIG. 2. Feynman diagrams contributing to first order bremsstrahlung radiation cross section.

These four matrix elements refer to the emission of a photon by the incident electron, scattered electron, incident proton, and scattered proton respectively. To evaluate them, one requires a knowledge of the coupling of the electron and proton to the photon. The electron coupling is given exactly by QED and is specified by the electron current

$$J_e^\mu(q)=e\bar{u}_e(k+q)\gamma^\mu u_e(k). \tag{9}$$

Here $e=-\sqrt{4\pi\alpha}$ is the electron charge and u_e is the electron spinor, normalized to $\bar{u}_e(k)u_e(k)=2m$ (m is the electron mass). The proton-photon coupling is complicated by the fact that the proton is in general bound and off-shell, and the description of such a proton is only approximately known [12]. For the present, we neglect these effects and discuss elastic scattering from an on-shell proton:

$$J_p^\mu(q)=-e\bar{u}_p(p+q)\Gamma^\mu(q)u_p(p). \tag{10}$$

The deviation of the proton from a point particle is described by

$$\Gamma^\mu(q)=F_1(q^2)\gamma^\mu+\frac{1}{2M}F_2(q^2)i\sigma^{\mu\nu}q_\nu, \tag{11}$$

using the free proton form factors. Again, the proton spinor is normalized to the proton mass: $\bar{u}_p(k)u_p(k)=2M$. Using these couplings, one obtains the following expressions for the first-order bremsstrahlung matrix elements:

$$\mathcal{M}_{\rm ei}=i\bar{u}_e(k')\gamma^\mu\left[\frac{i\gamma^\nu(k_\nu-\omega_\nu)+m}{(k-\omega)^2-m^2}\right]\times e\gamma^\nu\varepsilon_\nu u_e(k)\frac{e^2}{q_p^2-\mu^2}\bar{u}_p(p')\Gamma_\mu(q_p)u_p(p),$$

$$\mathcal{M}_{\rm ef}=i\bar{u}_e(k')e\gamma^\nu\varepsilon_\nu\left[\frac{i\gamma^\nu(k'_\nu+\omega_\nu)+m}{(k'+\omega)^2-m^2}\right]\times\gamma^\mu u_e(k)\frac{e^2}{q_p^2-\mu^2}\bar{u}_p(p')\Gamma_\mu(q_p)u_p(p),$$

$$\mathcal{M}_{\rm pi}=i\bar{u}_p(p')\Gamma^\mu(q)\left[\frac{i\gamma^\nu(p_\nu-\omega_\nu)+M}{(p-\omega)^2-M^2}\right]\times(-e)\Gamma^\nu(\omega)\varepsilon_\nu u_p(p)\frac{e^2}{q^2-\mu^2}\bar{u}_e(k')\gamma_\mu u_e(k),$$

$$\mathcal{M}_{\rm pf}=i\bar{u}_p(p')(-e)\Gamma^\nu(\omega)\varepsilon_\nu\left[\frac{i\gamma^\nu(p'_\nu+\omega_\nu)+M}{(p'+\omega)^2-M^2}\right]\times\Gamma^\mu(q)u_p(p)\frac{e^2}{q^2-\mu^2}\bar{u}_e(k')\gamma_\mu u_e(k). \tag{12}$$

Here ε_ν is the polarization of the bremsstrahlung photon, $q_p=p'-p$ is the momentum transferred to the proton if the electron emits the photon, and $q=k-k'$ is the momentum transferred to the proton if the proton emits the photon. Also, μ is a parameter representing the photon mass, which will ultimately be taken to 0. The single ambiguity in Eq. (12) is the assumption that the intermediate proton propagates like a Dirac particle and that there are no contributions from excited hadronic states. This should be a good approximation for small photon energies.

The single photon emission cross section can be calculated from these expressions, with no further approximations. However, the formulas simplify greatly in the limit that the photon energy ω^0 is much less than the momenta of the initial and final state fermions. In this case, the basic one-photon exchange (Born) amplitude $\mathcal{M}_{ep}^{(1)}$ factorizes from the bremsstrahlung amplitudes, giving

$$\mathcal{M}_{\rm ei}=e\mathcal{M}_{ep}^{(1)}\left(\frac{-\varepsilon\cdot k}{\omega\cdot k}\right),$$

$$\mathcal{M}_{\rm ef}=e\mathcal{M}_{ep}^{(1)}\left(\frac{\varepsilon\cdot k'}{\omega\cdot k'}\right),$$

$$\mathcal{M}_{\rm pi}=-e\mathcal{M}_{ep}^{(1)}\left(\frac{-\varepsilon\cdot p}{\omega\cdot p}\right),$$

$$\mathcal{M}_{\rm pf}=-e\mathcal{M}_{ep}^{(1)}\left(\frac{\varepsilon\cdot p'}{\omega\cdot p'}\right). \tag{13}$$

This limit is referred to as the *soft photon approximation* (SPA); it can be seen to be reasonable from the distinctive $1/\omega$ energy dependence of the emission amplitudes. Part of this approximation is the use of the elastic (unradiated) values of the fermion momenta k, k', p, and p' in the above expressions. These elastic values are also used in the evaluation of the one-photon exchange amplitude,

$$\mathcal{M}_{ep}^{(1)} = i\bar{u}_e(k')\gamma^\mu u_e(k)\frac{e^2}{q^2-\mu^2}\bar{u}_p(p')\Gamma_\mu(q)u_p(p). \tag{14}$$

The resulting total cross section for single-photon bremsstrahlung is thus given by

$$\frac{d\sigma}{d\Omega_e d^3\omega} = \frac{d\sigma^{(1)}}{d\Omega_e}\bigg|_{ep}\frac{-\alpha}{4\pi^2\omega^0}\left[\frac{k'}{\omega\cdot k'}-\frac{p'}{\omega\cdot p'}-\frac{k}{\omega\cdot k}+\frac{p}{\omega\cdot p}\right]^2. \tag{15}$$

For later convenience, using $d^3\omega = \omega^{02}d\omega^0 d\Omega_\gamma$, we write this as a product of photon energy and angle distributions,

$$\frac{d\sigma}{d\Omega_e d\Omega_\gamma d\omega^0} = \frac{d\sigma^{(1)}}{d\Omega_e}\bigg|_{ep}\frac{A(\Omega_\gamma)}{\omega^0}, \tag{16}$$

where

$$A(\Omega_\gamma) = -\frac{\alpha\omega^{02}}{4\pi^2}\left[\frac{k'}{\omega\cdot k'}-\frac{p'}{\omega\cdot p'}-\frac{k}{\omega\cdot k}+\frac{p}{\omega\cdot p}\right]^2 \tag{17}$$

depends only on the photon direction $\hat{\omega}$. Integrating Eq. (15) over photon angle and energy, one obtains the cross section for emitting a photon of energy less than ΔE_m:

$$\frac{d\sigma}{d\Omega_e}(\omega^0<\Delta E_m) = \int_0^{\Delta E_m} d^3\omega\frac{d\sigma}{d\Omega_e d^3\omega} = \frac{d\sigma^{(1)}}{d\Omega_e}\bigg|_{ep}(-2\alpha)\sum_{i,j}\Theta(p_i)\Theta(p_j)\times B(p_i,p_j,\Delta E_m), \tag{18}$$

where

$$B(p_i,p_j,\Delta E_m) = \int_0^{\Delta E_m} d^3\omega\frac{1}{8\pi^2\omega^0}\frac{p_i\cdot p_j}{(\omega\cdot p_i)(\omega\cdot p_j)}. \tag{19}$$

Here, two pieces of convenient notation have been introduced. p_i for $i=1,\ldots,4$ is used to represent the four fermion momenta k,k',p,p' in turn; the constants $\Theta(p_i)$ denote the signs accompanying each term, $\Theta(k)=\Theta(p')=-1$ and $\Theta(k')=\Theta(p)=1$. This integral can be evaluated using the expression

$$\omega\cdot k = \omega(\epsilon - |\mathbf{k}|\cos\theta), \tag{20}$$

as well as introducing a new variable x as indicated in Eq. (III.19) of Tsai [4]:

$$p_x = xp_i + (1-x)p_j. \tag{21}$$

One then obtains

TABLE II. Ratio of single photon bremsstrahlung cross section calculated in the soft photon approximation to the full calculation, at $Q^2=1$ $(\mathrm{GeV}/c)^2$. Various photon energies ω^0 are considered; the photon angle is taken to be in the direction of either the initial (i) or final (f) electron. The values in parentheses are the SPA/full ratios using a pointlike proton in the calculations.

ω^0 (MeV)	i	f
1	1.0023 (1.0002)	0.9993 (0.9993)
10	1.023 (1.002)	0.993 (0.993)
100	1.26 (1.02)	0.93 (0.93)
200	1.59 (1.04)	0.87 (0.87)

$$B(p_i,p_j,\Delta E_m) = \frac{p_i\cdot p_j}{2\pi}\int_0^1 dx\int_0^{\Delta E_m}\frac{\omega^2 d\omega}{\omega^0}\frac{1}{p_x^2\omega^2+\mu^2(p_x^0)^2} = \frac{p_i\cdot p_j}{2\pi}\int_0^1 dx\frac{1}{p_x^2}\ln\left(\frac{\Delta E_m}{p_x^0}\right)+\frac{1}{2p_x^2}\ln\left(\frac{p_x^2}{\mu^2}\right) + \frac{p_x^0-|\mathbf{p}_x|}{2|\mathbf{p}_x|}\ln\left(\frac{p_x^0-|\mathbf{p}_x|}{p_x^0+|\mathbf{p}_x|}\right)+\ln\left(\frac{2p_x^0}{p_x^0+|\mathbf{p}_x|}\right). \tag{22}$$

We note that the sum $\Sigma_{i,j}\Theta(p_i)\Theta(p_j)B(p_i,p_j,\Delta E_m)$ is negative, making the total cross section [and the angular distribution $A(\hat{\omega})$] positive.

One observes that this expression contains two nonphysical divergences: when the "photon mass" $\mu\to 0$ and when the energy cutoff $\Delta E_m\to 0$. Both of these are due to approximations made so far, and will be addressed in later sections. Before continuing, however, it is worthwhile to try to evaluate the validity of the soft photon approximation. As mentioned above, the one photon bremsstrahlung calculation can be computed without this approximation. Accordingly, the ratio of the full to the soft photon calculation is presented in Table II for $-q^2=Q^2=1$ $(\mathrm{GeV}/c)^2$ and a variety of photon energies, and in Table III for a photon energy of 100 MeV and a range of Q^2 from 1 to 15 $(\mathrm{GeV}/c)^2$. Qualitatively, one sees that the SPA improves at low photon energies and high momentum transfers, as expected. At $Q^2=1$ $(\mathrm{GeV}/c)^2$, the discrepancy between the two calculations is less than 1% for photon energies less than 10 MeV, while for a photon energy of 100 MeV the discrepancy drops

TABLE III. Ratio of single photon bremsstrahlung cross section calculated in the soft photon approximation to the full calculation, for photon energy $\omega^0=100$ MeV. Various momentum transfers Q^2 are considered; the photon angle is taken to be in the direction of either the initial (i) or final (f) electron.

Q^2 $(\mathrm{GeV}/c)^2$	i	f
1	1.26	0.93
5	1.14	0.93
9	1.05	0.99
15	1.03	0.99

to 5% at $Q^2=9$ $(\mathrm{GeV}/c)^2$. The discrepancies are considerably higher at the other settings listed, however. Two effects are involved: the shape of the bremsstrahlung energy spectrum, and the evaluation of the matrix elements using elastic ($\omega^0=0$) particle vectors [i.e., neglecting the difference between q and q in Eq. (12)]. In an attempt to separate these effects, Table II also contains the SPA to full ratio using a pointlike proton, i.e., a proton whose form factors are $G_E^p(Q^2)=1$ and $G_M(Q^2)=\mu_p$ (these are the $Q^2=0$ values of the form factors of the physical proton).At $Q^2=1$ $(\mathrm{GeV}/c)^2$, one sees that most of the discrepancy is due to the q-dependent form factors. To correct this one must evaluate the cross section using a value of q which is corrected for the effect of radiation. In other words, one must distinguish between photons emitted before and after the hard scattering, a task which is complicated by the interference terms between the Bremsstrahlung amplitudes $\mathcal{M}_{\mathrm{ei}}$, $\mathcal{M}_{\mathrm{ef}}$, $\mathcal{M}_{\mathrm{pi}}$, and $\mathcal{M}_{\mathrm{pf}}$. However, such a correction can be built into the calculation, as is explained later on. The maximal E_m range below pion production threshold is about 140 MeV, so the $\omega^0=100$ MeV results in Table II can be considered a typical worst case. Assuming that the correction to q at the hard scattering vertex can be accomplished, one is faced with a SPA inaccuracy of at most 2% for radiation in the direction $\hat{k}$ and 7% for radiation in the direction $\hat{k}'$. We point out in passing that these discrepancies are given as fractions of the radiative *corrections*, which are themselves small; the effect of these discrepancies on the final cross section is thus much less than the quoted percentages. Nonetheless, the effect may be of relevance for precision measurements.

B. Virtual photon corrections

One of the nonphysical divergences observed in Eq. (22) was found in the limit $\mu\to 0$. This is known as an ''infrared divergence,'' and is a direct consequence of the fact that the one photon bremsstrahlung cross section is of order α^3 and that other diagrams of the same order have not been included yet. These are amplitudes for the exchange of two virtual photons, collectively referred to as $\mathcal{M}_{ep}^{(2)}$. These must be summed coherently with $\mathcal{M}_{ep}^{(1)}$, which represents the same final state:

$$\mathcal{M}_{ep}^{\,2}=|\mathcal{M}_{ep}^{(1)}|^2+\mathcal{M}_{ep}^{(2)\dagger}\mathcal{M}_{ep}^{(1)}+\mathcal{M}_{ep}^{(1)\dagger}\mathcal{M}_{ep}^{(2)}+\mathcal{O}(\alpha^4). \tag{23}$$

Figure 3 contains a summary of the second-order amplitudes. Unfortunately, several of these depend implicitly on the strong interaction via the poorly known proton current. The point of view advocated by Mo and Tsai and espoused here, is to include only those terms which do not unambiguously depend on the strong interaction. Certain amplitudes such as $\mathcal{M}_{ep}^{(2.3)}$ in the figure *are* calculated, but only infrared divergent terms necessary to cancel those from the bremsstrahlung cross section are kept; the rest are left buried in the electron-proton cross section. It should be noted that other workers [7] have derived alternative expressions for the virtual radiative correction, by including some of the components left out

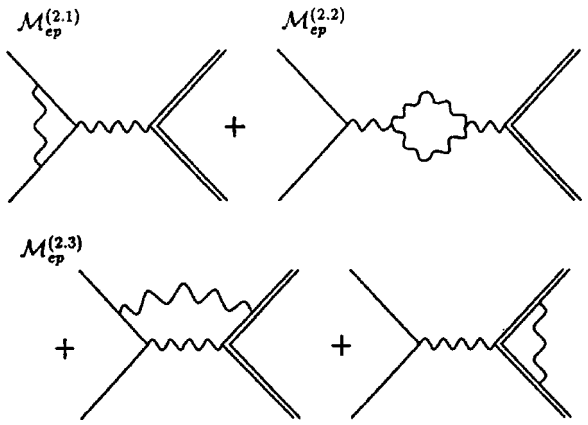

FIG. 3. Feynman diagrams representing virtual photon corrections to one-photon exchange ep cross section included here and in Ref. [4].

by Mo and Tsai. However, the point to be made here is that the evaluation of $\mathcal{M}_{ep}^{(1)}$ includes the use of proton form factors extracted from *previous* data. The radiative corrections applied should thus be *consistent* with whatever corrections were used in extracting these form factors [13,14]. The standard prescription given by Eq. II.6 of Mo and Tsai [6] is thus the appropriate choice, with the addition of the Schwinger correction and vacuum polarization from quark and heavy lepton loops [13,15].

The second order diagrams depicted in Fig. 3 are grouped into three categories depending on their sensitivity to the strong interaction. We use the same evaluation of these amplitudes as Mo and Tsai, and restate them here. Also used is the notation

$$K(p_i,p_j)=p_i\cdot p_j\int_0^1\frac{dx}{p_x^2}\ln\left(\frac{p_x^2}{\mu^2}\right), \tag{24}$$

describing the form of the infrared divergent terms. Note that

$$K(p_i,p_i)=\ln\left(\frac{m_i^2}{\mu^2}\right), \tag{25}$$

and that the IR divergent term of Eq. (22) has this form.

The electron-photon vertex correction $\mathcal{M}_{ep}^{(2.1)}$ is known exactly from QED. In the limit $Q^2\gg m^2$ (which is well satisfied by momentum transfers in the GeV/c range), one obtains

$$\mathcal{M}_{ep}^{(2.1)}=\frac{\alpha}{2\pi}\left[-K(k,k')+\ln\left(\frac{m^2}{\mu^2}\right)+\frac{3}{2}\ln\left(\frac{-q^2}{m^2}\right)-2\right]\mathcal{M}_{ep}^{(1)}. \tag{26}$$

The vacuum polarization correction, $\mathcal{M}_{ep}^{(2.2)}$, contains contributions from both lepton and hadronic loops. The former are known unambiguously from QED, the latter are calculated in a similar manner. They contribute

$$\mathcal{M}_{ep}^{(2.2)}=\alpha\left[\sum_i\ \delta_i^{\mathrm{vp}}\right]\mathcal{M}_{ep}^{(1)}, \tag{27}$$

where

$$\delta_i^{\rm vp}=\frac{1}{3\pi}\left(-\frac{5}{3}-\frac{4m_i^2}{q^2}+\left(1+\frac{2m_i^2}{q^2}\right)\sqrt{1-\frac{4m_i^2}{q^2}}\times\log\left[\frac{1+\sqrt{1-\frac{4m_i^2}{q^2}}}{\sqrt{1-\frac{4m_i^2}{q^2}}-1}\right]\right) \tag{28}$$

and Σ_i sums over the different flavors of leptons and light quarks with mass m_i. In the limit $Q^2 \gg m^2$ one obtains

$$\delta_i^{\rm vp}=\frac{1}{3\pi}\left[-\frac{5}{3}+\ln\left(\frac{-q^2}{m_i^2}\right)\right]. \tag{29}$$

As there are no IR divergent terms in the vacuum polarization amplitude, further contributions from the strong interaction are neglected. Finally, $\mathcal{M}_{ep}^{(2.3)}$ includes two-photon exchange and nucleon self-energy graphs, both of which depend intrinsically on the strong interaction. Only the IR divergent terms are used:

$$\mathcal{M}_{ep}^{(2.3)}=\frac{\alpha}{2\pi}\left[K(k,p)+K(k',p')-K(k',p)-K(k,p')-K(p,p')-\ln\left(\frac{M^2}{\mu^2}\right)\right]. \tag{30}$$

The total cross section for emitting a photon with energy less than ΔE_m is now obtained by adding all of these terms to Eq. (18). The dependence on the photon mass cancels as required, leaving

$$\frac{d\sigma}{d\Omega_e}(\omega^0<\Delta E_m)=\left.\frac{d\sigma^{(1)}}{d\Omega_e}\right|_{ep}(1-\delta_{\rm soft}(\Delta E_m)-\delta_{\rm hard}), \tag{31}$$

where

$$\delta_{\rm soft}(\Delta E_m)=2\alpha\sum_{i,j}\Theta(p_i)\Theta(p_j)\bar{B}(p_i,p_j,\Delta E_m) \tag{32}$$

and

$$\delta_{\rm hard}=2\alpha\left[-\frac{3}{4\pi}\ln(-q^2/m^2)+\frac{1}{\pi}-\sum_i\delta_i^{\rm vp}(q^2)\right]. \tag{33}$$

Here, $d\sigma^{(1)}/d\Omega_e|_{ep}$ represents the one-photon exchange *ep* cross section, $\delta_{\rm hard}$ is the contribution from the second order virtual photon diagrams, and $\delta_{\rm soft}(\Delta E_m)$ is due to one photon bremsstrahlung. $\bar{B}(p_i,p_j,\Delta E_m)$ is simply $B(p_i,p_j,\Delta E_m)$ of Eq. (22) without the IR divergent term. The subscript ''hard'' refers to the dominance of high momentum virtual photons in the $\delta_{\rm hard}$ correction after cancellation of the IR divergences. The subscript ''soft'' refers to the assumption $\omega^0 < \epsilon, \epsilon'$ used in the derivation of $\delta_{\rm soft}$ (cf. the SPA in Sec. III A).

TABLE IV. Values for the radiative correction functions δ, evaluated at various momentum transfers and for cutoff photon energies of 10 and 140 MeV. Note that the virtual correction $\delta_{\rm hard}$ is independent of this cutoff parameter. Note also that the results depend on the choice of electron scattering angle as well as on Q^2. The final column is the percentage contribution of the proton-proton and electron-proton interference terms to the total bremsstrahlung correction $[(\delta_{\rm soft}^{ep}+\delta_{\rm soft}^{pp})/\delta_{\rm soft}]$.

Q^2 $(\mathrm{GeV}/c)^2$	ΔE_m (MeV)	$\delta_{\rm hard}$	$\delta_{\rm soft}^{ee}$	$\delta_{\rm soft}^{ep}$	$\delta_{\rm soft}^{pp}$	$\delta_{\rm soft}$	$p_{\rm soft}^{ep+pp}$ %
1	10	−0.07	0.332	0.015	0.007	0.354	6.2
	140		0.158	0.007	0.003	0.169	5.9
3	10	−0.08	0.377	0.038	0.019	0.434	13.1
	140		0.190	0.020	0.009	0.219	13.2
5	10	−0.08	0.398	0.056	0.028	0.482	17.4
	140		0.205	0.030	0.014	0.249	17.7
7	10	−0.09	0.424	0.070	0.035	0.529	19.8
	140		0.226	0.038	0.019	0.283	20.1
6	10	−0.09	0.519	0.019	0.032	0.569	9.0
	140		0.323	0.011	0.017	0.351	8.0
9	10	−0.09	0.545	0.024	0.041	0.610	10.7
	140		0.345	0.014	0.022	0.382	9.4
12	10	−0.09	0.564	0.028	0.049	0.641	12.0
	140		0.360	0.017	0.028	0.405	11.1
15	10	−0.09	0.579	0.032	0.056	0.667	13.2
	140		0.372	0.020	0.032	0.424	12.3

In order to separate out the contribution of the proton we divide $\delta_{\rm soft}(\Delta E_m)$ into three parts,

$$\delta_{\rm soft}(\Delta E_m)=\delta_{\rm soft}^{ee}(\Delta E_m)+\delta_{\rm soft}^{ep}(\Delta E_m)+\delta_{\rm soft}^{pp}(\Delta E_m). \tag{34}$$

$\delta_{\rm soft}^{ee}$ is the electron bremsstrahlung contribution, involving $\bar{B}(k,k,\Delta E_m)$, $\bar{B}(k',k',\Delta E_m)$, and $-2\bar{B}(k,k',\Delta E_m)$. $\delta_{\rm soft}^{ep}$ includes the electron-proton interference terms $-2\bar{B}(k,p,\Delta E_m)$, $2\bar{B}(k,p',\Delta E_m)$, $2\bar{B}(k',p,\Delta E_m)$, and $-2\bar{B}(k',p',\Delta E_m)$; while $\delta_{\rm soft}^{pp}$ is entirely due to proton radiation and includes the remaining terms $\bar{B}(p,p,\Delta E_m)$, $\bar{B}(p,p',\Delta E_m)$, and $-2\bar{B}(p',p',\Delta E_m)$. Table IV contains values of these terms as well as $\delta_{\rm hard}$ at various kinematics. Note that $\delta_{\rm hard}$ is negative, and so causes a net *increase* in the total *ep* cross section. Its magnitude is also small: less than 10% up to Q^2 of 15 $(\mathrm{GeV}/c)^2$. The direct proton contribu-

tion $\delta_{\rm soft}^{pp}$ varies from 2% (lowest Q^2) to 10% (highest Q^2) of the electron contribution $\delta_{\rm soft}^{ee}$. The electron-proton interference is about twice the size of the direct proton term for the first four kinematics, leading to a net 6–20 % contribution of proton bremsstrahlung, but only about half the size of the direct proton term for the last four kinematics. This is governed by the ratio of ϵ' to ϵ ($\delta_{\rm soft}^{ep}$ is zero in the limit $\epsilon' = \epsilon$). From Table IV it is clear that proton radiation, though afflicted by strong interaction uncertainties, cannot be neglected at large momentum transfer.

A complete evaluation of the functions $\overline{B}(p_i, p_j, \Delta E_m)$, and thus of Eq. (32), is often done numerically. However, analytic evaluation is possible, as outlined in the Appendix. In general, numerous Spence functions Φ must be computed, where

$$\Phi(x) = \int_0^x \frac{-\ln(|1-y|)}{y} dy. \tag{35}$$

As an aside, the contributions of these functions turn out to be important only when their arguments are large ($|x| \gg 1$), and in this case an excellent approximation is provided by

$$\Phi(x) \cong \frac{1}{2}\ln^2(|x|). \tag{36}$$

The formulas for $\delta_{\rm soft}$ simplify, however, in the ''ultrarelativistic (UR) limit'' where the momentum transfer and vertex momentum of the final electron are large compared to both the nucleon and electron mass. In this limit, one obtains the following closed forms:

$$\delta_{ee}^{\rm ur} = \frac{\alpha}{\pi}\ln\left(\frac{kk'}{(\Delta E_m)^2}\right)\left[\ln\left(\frac{-q^2}{m^2}\right) - 1\right],$$

$$\delta_{pp}^{\rm ur} = \frac{Z^2\alpha}{\pi}\left[\ln\left(\frac{p^0 p^{0'}}{(\Delta E_m)^2}\right)\left[\ln\left(\frac{-q^2}{M^2}\right) - 1\right] + \frac{1}{2}\ln^2\left(\frac{p^{0'}}{M}\right)\right],$$

$$\delta_{ep}^{\rm ur} = \frac{Z\alpha}{\pi}\left[\ln\left(\frac{p^0 p^{0'}}{\Delta E_m^2}\right)\ln\left(\frac{k}{k'}\right) + \ln\left(\frac{kk'}{\Delta E_m^2}\right)\ln\left(\frac{k}{k'}\right) + \frac{1}{2}\ln\left(\frac{kk'}{M^2}\right)\ln\left(\frac{k}{k'}\right)\right]. \tag{37}$$

The atomic number Z is retained in these forms to remind the reader that the results are also valid for electron-nucleus scattering, barring the neglect of earlier mentioned off-shell effects. Furthermore, this allows for easy differentiation between contributions involving the electron bremsstrahlung ($\sim Z^0$), the electron-proton interference ($\sim Z^1$), and the proton bremsstrahlung terms ($\sim Z^2$). These forms reveal the essential features of one-photon emission: all of the dependence of $\delta_{\rm soft}(\Delta E_m)$ on ΔE_m takes the form $\ln(1/\Delta E_m)$, but additional terms independent of the photon energy cutoff are also present. These expressions will prove very useful later on, and so it is worthwhile to see how good the UR approximation is. A comparison of $\delta_{\rm soft}(\Delta E_m)$ computed using Eq. (22) and Eq. (37) is presented in Table V. One sees that in the chosen kinematics the approximation is accurate to at least 2%. This is because the electrons are always highly relativistic and the contribution to δ due to the final nucleon is small when nonrelativistic. The nucleon contribution becomes significant only when relativistic (it is equal to the electron's in the very high energy limit) and in that case Eq. (37) provides a good approximation.

TABLE V. Single photon bremsstrahlung spectrum, evaluated at several kinematic settings and integrated up to photon energies of 10 and 140 MeV. $\delta_{\rm soft}$ is calculated using the full SPA expressions of Eq. (22); $\delta_{\rm soft}^{\rm ur}$ is from the closed form expressions of Eq. (37) found in the ultrarelativistic limit. The final column presents the percentage discrepancy of the UR calculation relative to the full SPA.

Q^2 $(\mathrm{GeV}/c)^2$	ΔE_m (MeV)	$\delta_{\rm soft}$	$\delta_{\rm soft}^{\rm ur}$	Discrep. %
1	10	0.354	0.347	−2.0
	140	0.169	0.166	−1.8
5	10	0.482	0.474	−1.7
	140	0.249	0.246	−1.2
9	10	0.610	0.609	−0.2
	140	0.382	0.383	0.3
15	10	0.667	0.668	0.2
	140	0.424	0.427	0.7

It is worthwhile to compare our results, given by Eqs. (32) and (33) with those of Mo and Tsai (Eq. II.6), denoted δ_{MT}. The only difference between the two calculations is that our calculation integrates the photon emission up to a maximum photon energy of ΔE_m (corresponding to a missing energy of ΔE_m), while the calculation by Mo and Tsai integrates over all photons corresponding to an energy loss of less than $\Delta\epsilon'$. The two calculations are equal only in the limit that the proton mass is large in which case the electron energy loss equals the energy of the emitted photon. In general, for finite proton mass, photon emission additionally affects the recoil energy, and thus the energy of the emitted photon is greater than the electron energy loss. This implies that the calculation by Mo and Tsai at a given value of $\Delta\epsilon'$ contains also contributions of additional photons with energies ΔE_m larger than $\Delta\epsilon'$. The degree to which this energy can be different is determined by the ratio of ϵ to ϵ'. Table VI compares the results of both calculations. As expected from the previous discussion it is always true that

$$\delta_{MT}(\Delta\epsilon' = \Delta E) \leqslant \delta(\Delta E_m = \Delta E) = \delta_{hard} + \delta_{soft}(\Delta E_m = \Delta E), \tag{38}$$

where the largest difference occurs when ϵ is far larger than ϵ'.

TABLE VI. Comparison of δ with δ_{MT} and δ_{Schw} at various kinematics with $\omega^0=10$ MeV.

Q^2 $(\mathrm{GeV}/c)^2$	δ	δ_{MT}	δ_{Schw}
1	0.284	0.266	0.277
5	0.402	0.315	0.363
9	0.520	0.496	0.478
15	0.577	0.542	0.517

Similarly, to revisit the role the proton is playing, it is useful to contrast our formulas with the Schwinger formula [2] that ignores proton recoil and radiation,

$$\delta_{Schw}=\frac{2\alpha}{\pi}\left[\ln\left(\frac{k}{\Delta E}\right)-\frac{13}{12}\right]\left[\ln\left(\frac{-q^2}{m^2}\right)-1\right]+\frac{17}{36}. \quad (39)$$

Table VI verifies that the Schwinger correction, in its simplicity, gives a fairly good approximation of our results, that only gradually becomes worse at higher energies. This is due to the overestimate of the electron bremsstrahlung contribution in the Schwinger correction, partly compensating the positive contribution of the proton radiation.

C. Higher order bremsstrahlung

In the previous section, we removed the infrared divergence from the first order bremsstrahlung cross section. The other divergence that needs to be understood also occurs in the limit $\Delta E_m\to 0$: the number of photons emitted becomes infinite as $\omega\to 0$. In other words, the first order perturbation expansion breaks down as ΔE_m becomes very small, and one must include the possibility to emit many soft photons. In actuality, the probability of scattering without losing any energy to bremsstrahlung is zero so the actual cross section approaches zero as $\Delta E_m\to 0$.

It was originally determined by Yennie, Frautschi, and Suura (Ref. [3]) that the emission of soft photons can be summed to all orders via exponentiation:

$$\frac{d\sigma}{d\Omega_e}(\omega_i^0<\Delta E_m)=\left.\frac{d\sigma^{(1)}}{d\Omega_e}\right|_{ep} e^{-\delta_{\mathrm{soft}}(\Delta E_m)}(1-\delta_{\mathrm{hard}}). \quad (40)$$

The notation (ω_i^0) indicates that this expression represents the cross section for emitting any number of soft photons, *each* with energy less than ΔE_m. In practice, however, one is interested in the *total* photon energy emitted. This case is discussed in the remainder of this section, and found to agree with the preceding formula to within a correction of order α^2.

Recall that the probability for emitting a single bremsstrahlung photon has a $1/\omega^0$ energy dependence that factors from the angular distribution $A(\hat{\omega})$ [Eq. (16)]. In order to maintain a handle on the $\Delta E_m\to 0$ divergence for the moment, we write the cross section to emit one photon with energy $\omega_1^0>E_0$, along with any number of photons each with energy less than E_0:

$$\frac{d\sigma}{d\Omega_e d\omega_1^0 d\Omega_1}(n=1,E_0)=\left.\frac{d\sigma^{(1)}}{d\Omega_e}\right|_{ep} e^{-\delta_{soft}(E_0)}(1-\delta_{\mathrm{hard}})\frac{A(\hat{\omega}_1)}{\omega_1^0}\theta(\omega_1^0-E_0). \quad (41)$$

Here, θ is the usual step function, and $d\Omega_1$ indicates the emission angle of the photon ω_1. Similarly, the cross section to emit *two* photons with energy $\omega_1^0>E_0$ and $\omega_2^0>E_0$, along with any number of photons with individual energy less than E_0 is

$$\frac{d\sigma}{d\Omega_e d\omega_1^0 d\Omega_1 d\omega_2^0 d\Omega_2}(n=2,E_0)=\left.\frac{d\sigma^{(1)}}{d\Omega_e}\right|_{ep} e^{-\delta_{\mathrm{soft}(E_0)}}(1-\delta_{\mathrm{hard}})\times\frac{1}{2}\frac{A(\hat{\omega}_1)}{\omega_1^0}\theta(\omega_1^0-E_0)\times\frac{A(\hat{\omega}_2)}{\omega_2^0}\theta(\omega_2^0-E_0). \quad (42)$$

Generalizing this to the case of n photons of ''large'' energy, one obtains

$$\frac{d\sigma}{d\Omega_e d\omega_1^0 d\Omega_1\cdots d\omega_n^0 d\Omega_n}(n,E_0)=\left.\frac{d\sigma^{(1)}}{d\Omega_e}\right|_{ep} e^{-\delta_{\mathrm{soft}}(E_0)}(1-\delta_{\mathrm{hard}})\frac{1}{n!}\frac{A(\hat{\omega}_1)}{\omega_1^0}\times\theta(\omega_1^0-E_0)\cdots\frac{A(\hat{\omega}_n)}{\omega_n^0}\theta(\omega_n^0-E_0). \quad (43)$$

The differential cross section for emitting a *total* energy $\Sigma_i\omega_i^0=E_{tot}$ can be determined by multiplying the above with a delta function and integrating over individual photon energies. Also, we sum over all numbers n of emitted photons:

$$\frac{d\sigma}{d\Omega dE_{tot}}(E_0)=\sum_{n=0}^{\infty}\int_{E_0}^{E_{tot}}d\omega_1^0 d\Omega_1\cdots\int_{E_0}^{E_{tot}}d\omega_n^0 d\Omega_n\times\frac{d\sigma}{d\Omega_e d\omega_1^0 d\Omega_1\cdots d\omega_n^0 d\Omega_n}(n,E_0)\times\delta(\omega_1^0+\cdots+\omega_n^0-E_{tot}). \quad (44)$$

One observes that the angular integration can be done at once for each photon, and for convenience we write

$$\lambda=\int d\Omega_\gamma A(\hat{\omega}). \quad (45)$$

We then combine Eqs. (43) and (44) to obtain

$$\frac{d\sigma}{d\Omega dE_{tot}}(E_0)=\frac{d\sigma^{(1)}}{d\Omega_e}\bigg|_{ep} e^{-\delta_{\rm soft}(E_0)}(1-\delta_{\rm hard}) \times\sum_{n=0}^{\infty}\frac{1}{n!}\left(\prod_{i=1}^{n}\int_{E_0}^{E_{tot}} d\omega_i^0\frac{\lambda}{\omega_i^0}\right) \times\delta(\omega_1^0+\cdots+\omega_n^0-E_{tot}). \quad (46)$$

This is a form that we will encounter again later on. It can be evaluated by substituting an integral form for the delta function:

$$\delta\left(\sum_i \omega_i^0-E_{tot}\right)=\frac{1}{2\pi}\int_{-\infty}^{\infty}e^{ix(\sum_i \omega_i^0-E_{tot})}dx, \quad (47)$$

which gives Eq. (46) the familiar form $\Sigma_{n=0}^{\infty}(z^n/n!)=e^z$. Carrying through the computation, one finds that the $E_0\rightarrow 0$ divergence in $e^{-\delta_{\rm soft}(E_0)}$ is canceled by the similar terms due to the E_0 lower integration limit. Taking the limit $E_0\rightarrow 0$, the following relatively simple form is obtained:

$$\frac{d\sigma}{d\Omega_e dE_{tot}}=\frac{d\sigma^{(1)}}{d\Omega_e}\bigg|_{ep}(1-\delta_{\rm hard})(-\delta'_{\rm soft}(E_{tot}))e^{-\delta_{\rm soft}(E_{tot})}F(\lambda). \quad (48)$$

The function $F(\lambda)$ is expressed in terms of the gamma function and Euler's constant $C\cong 0.577$; if we recall that λ is of order α, we can expand this function in powers of λ:

$$F(\lambda)=\frac{e^{-C\lambda}}{\Gamma(1+\lambda)}=1-\frac{\pi^2\lambda^2}{12}+\cdots. \quad (49)$$

Our main result for the higher order bremsstrahlung case is summarized in Eq. (48), (45), and (49). Additionally, one can obtain the cross section for total emitted energy less than ΔE_m by integrating Eq. (48) from $E_{tot}=0$ to $E_{tot}=\Delta E_m$:

$$\frac{d\sigma}{d\Omega}\left(\sum\omega^0<\Delta E_m\right)=\left|\frac{d\sigma^{(1)}}{d\Omega_e}\right|_{ep}(1-\delta_{\rm hard})e^{-\delta_{\rm soft}(\Delta E_m)}[1+\mathcal{O}(\alpha^2)]. \quad (50)$$

This agrees with the previous exponentiated formula, Eq. (40), to within a correction of order α^2.

Exponentiating $\delta_{\rm soft}$ thus provides a good approximation to the bremsstrahlung cross section for emitting a *total* photon energy up to a certain cutoff value. The exponentiated cross section also has the correct limiting behavior, $\lim_{\Delta E_m\rightarrow 0}(d\sigma/d\Omega_e)(\Sigma\omega^0<\Delta E_m)=0$, since $\delta_{soft}(\Delta E_m)\sim\overline{B}(p_i,p_j,\Delta E_m)\sim\ln(\Delta E_m)$. Note, however, that $\delta_{\rm hard}$ is *not* exponentiated. Mo and Tsai [6] take the point of view that whether or not to exponentiate this term is an open question. As with the choice of which second order diagrams to include in $\delta_{\rm hard}$, the crux of the matter is that experiments comparing results with one another must use the *same* prescription. In the case of $\delta_{\rm hard}$, however, this is generally a moot point since the correction itself is small: $\delta_{\rm hard}$ varies from 0.07 to 0.09, and so the difference between $(1-\delta_{\rm hard})$ and $e^{-\delta_{\rm hard}}$ is at most 0.4%.

TABLE VII. Importance of multiphoton emission on radiative correction factors for various kinematics and three values of total photon energy emitted.

Q^2 $(\mathrm{GeV}/c)^2$	ΔE_m (MeV)	$\exp(-\delta_{soft})(1-\delta_{hard})$	$1-\delta_{soft}-\delta_{hard}$
1	1	0.638	0.554
	10	0.750	0.716
	100	0.882	0.877
7	1	0.519	0.347
	10	0.642	0.561
	100	0.796	0.776
15	1	0.453	0.212
	10	0.560	0.423
	100	0.692	0.635

In Table VII we compare as a numerical example the first order and the exponentiated radiative corrections for various kinematics and total photon energies emitted. As one can see the difference can be quite noticable, supporting the findings of [8], where the inclusion of multiphoton emission showed a drastic improvement in the agreement between ^{3}He$(e,e'p)$ data and a Monte Carlo simulation. As expected, this difference grows especially large for small values of the total photon energy emitted. However, the effect can be as large as 10% up to a total photon energy of 100 MeV as Q^2 becomes as large as 15 $(\mathrm{GeV}/c)^2$. Likewise, multiphoton emission alters the radiative correction at the 10% level down to a photon energy ΔE_m of 1(10) MeV at the chosen kinematics for $Q^2=1(7)(\mathrm{GeV}/c)^2$. These are some relevant scales to keep in mind to deal with multiphoton emission when analyzing experimental data.

IV. PEAKING APPROXIMATIONS AND EXTERNAL BREMSSTRAHLUNG

A. Peaking approximations

We have now calculated the energy distribution for multiphoton bremsstrahlung to all orders, given the soft photon approximation and to within an order α^2 correction. However, to calculate radiative effects in a coincidence framework, one must know the effect of the emission cross section on *all* measured particle vectors. The integrated probability up to an energy cutoff is not enough, and one needs to know the angular distribution of photons as well.

The angular distribution of single photon bremsstrahlung is given by Eq. (17), and is plotted in Fig. 4 for $Q^2=1$, 7, and 15 $(\mathrm{GeV}/c)^2$. One salient feature of the distribution is immediately apparent: the radiation is strongly peaked along the directions of the incoming and outgoing electron. Only a

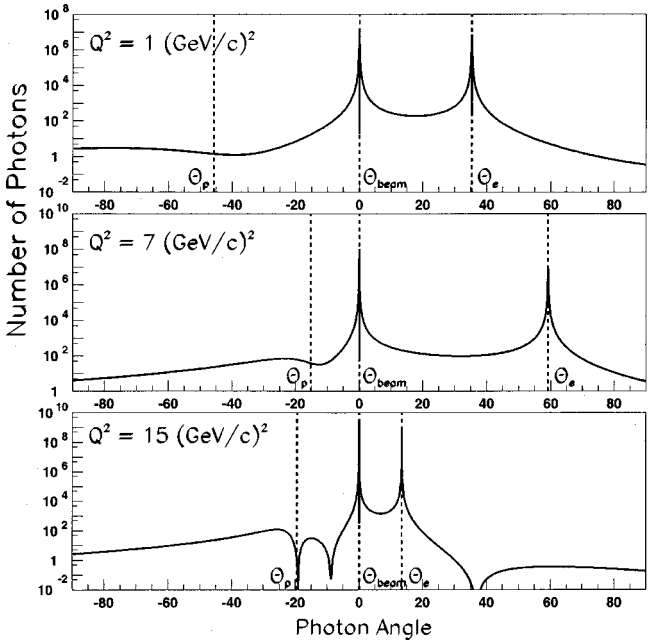

FIG. 4. Angular distribution of first order bremsstrahlung photons from Eq. (17), calculated at $Q^2=1,7$, and 15 $(\mathrm{GeV}/c)^2$ and showing the improvement in the peaking approximation with increasing momentum transfer. The photon angle is measured with respect to the direction of the incoming electron and given in degrees. The directions of the scattered electron and proton are indicated by dotted lines and the notation θ_e, θ_p.

very broad peak is seen in the direction of the scattered proton at $Q^2=1$ $(\mathrm{GeV}/c)^2$, but it becomes more sharply defined as Q^2 increases. These features suggest a simple approach to the angular distribution, known as the "peaking approximation:" the single photon bremsstrahlung spectrum may be divided into three discrete photon directions, along each of the vectors $\hat{k}$, $\hat{k}'$, and $\hat{p}'$. In other words, we replace $A(\hat{\omega})$ in Eq. (16) with the simple form

$$A_{\mathrm{peaking}}(\hat{\omega})=\lambda_e\delta(\hat{\omega}-\hat{k})+\lambda_{e'}\delta(\hat{\omega}-\hat{k}')+\lambda_{p'}\delta(\hat{\omega}-\hat{p}'), \tag{51}$$

where $\int d\Omega_\gamma\delta(\hat{\omega})=1$.

The terms of the exact one-photon angular distribution $A(\hat{\omega})$ may be divided into three groups, due to the electrons, the electron-proton interference, and the protons, respectively:

$$A(\hat{\omega})=-\frac{\alpha\omega^{02}}{4\pi^2}\left[\left(\frac{k'}{\omega\cdot k'}-\frac{k}{\omega\cdot k}\right)^2-2\left(\frac{k'}{\omega\cdot k'}-\frac{k}{\omega\cdot k}\right)\times\left(\frac{p'}{\omega\cdot p'}-\frac{p}{\omega\cdot p}\right)+\left(\frac{p'}{\omega\cdot p'}-\frac{p}{\omega\cdot p}\right)^2\right]. \tag{52}$$

In order to better understand the structure of the peaks, consider the expansion of the first term in a polar coordinate angle θ describing the direction of photon emission relative to the $\hat{k}$ direction. Using Eq. (20) one obtains, in the region $\theta\ll m/|\mathbf{k}|\ll 1$,

$$\omega^2\left(\frac{k'}{\omega\cdot k'}-\frac{k}{\omega\cdot k}\right)^2\sim 4\frac{|\mathbf{k}|^4}{m^4}\theta^2, \tag{53}$$

indicating that extremely close to the $\hat{k}$ peak, the emission probability actually drops to zero. This feature is too small to be seen in the electron peaks of Fig. 4, but is apparent in the much broader proton peak at $Q^2=15$ $(\mathrm{GeV}/c)^2$ (since $M/|\mathbf{p}'|$ is of order 10^{-1}). Further away from the peak, in the region $m/|\mathbf{k}|\ll\theta\ll 1$, the angular distribution falls off quadratically with θ:

$$\omega^2\left(\frac{k'}{\omega\cdot k'}-\frac{k}{\omega\cdot k}\right)^2\sim\frac{4}{\theta^2}. \tag{54}$$

This behavior is especially apparent in the electron peaks, where $m/|\mathbf{k}|$ is of order 10^{-4}. We will refer to this $1/\theta^2$ shape later on.

We next need to determine the values of λ_e, $\lambda_{e'}$, and $\lambda_{p'}$, by integrating the various terms of $A(\hat{\omega})$ and distributing the results among the three peaks. The first (electron) term of Eq. (52) produces two terms of the form

$$-\frac{\alpha\omega^{02}}{4\pi^2}\int d\Omega_\gamma\frac{k^2}{(\omega\cdot k)^2}=-\frac{\alpha}{\pi} \tag{55}$$

(one for each of k and k'). Since the integrand is highly peaked in the direction $\mathbf{k}$ (or $\mathbf{k}'$), it is assumed that all this strength contributes in the $\mathbf{k}$ (or $\mathbf{k}'$) direction. Next consider the integral of the cross term,

$$2\frac{\alpha\omega^{02}}{4\pi^2}\int d\Omega_\gamma\frac{k\cdot k'}{(\omega\cdot k)(\omega\cdot k')}. \tag{56}$$

In this case the integrand peaks in the $\mathbf{k}$ and $\mathbf{k}'$ directions. We evaluate it using

$$\begin{aligned}\int d\Omega_\gamma\frac{k\cdot k'}{(\omega\cdot k)(\omega\cdot k')}&\cong\int d\Omega_\gamma\frac{k\cdot k'}{(\omega\cdot k)(k\cdot k')}\frac{|\mathbf{k}|}{\omega^0}+\int d\Omega_\gamma\frac{k\cdot k'}{(k'\cdot k)(\omega\cdot k')}\frac{|\mathbf{k}'|}{\omega^0}\\&=\frac{2\pi}{\omega^2}\ln\left(\frac{\epsilon+|\mathbf{k}|}{\epsilon-|\mathbf{k}|}\right)+\frac{2\pi}{\omega^2}\ln\left(\frac{k'^0+|\mathbf{k}'|}{k'^0-|\mathbf{k}'|}\right).\end{aligned} \tag{57}$$

TABLE VIII. Comparison of the exact values (δ_{exact}) of radiative correction factors with the "typical" peaking approximation values (δ_{peak}) as given by Eq. (58), in the UR limit. The two additional columns indicate the main sources of the discrepancy as given by Eqs. (60) and (61).

Q^2 (GeV/c)^2	δ_{exact}	δ_{exact} - Δ	δ_{exact} - Δ - δ_{ep}	δ_{peak}
1	0.185	0.215	0.207	0.203
3	0.215	0.236	0.218	0.216
5	0.233	0.252	0.225	0.225
7	0.246	0.263	0.231	0.231
6	0.218	0.271	0.263	0.262
9	0.228	0.281	0.272	0.271
12	0.236	0.289	0.278	0.278
15	0.243	0.295	0.283	0.283

This expression approximately integrates over the two peaks separately; the first and second integrals are assumed to contribute to the $\mathbf{k}$ and $\mathbf{k}'$ peaks, respectively. Combining these equations, one obtains for $(\mathbf{k},\mathbf{k}')\gg 0$ the "typical" peaking approximation for electron bremsstrahlung:

$$\lambda_e=\frac{\alpha}{\pi}\left[\ln\left(\frac{4\mathbf{k}^2}{m^2}\right)-1\right],\quad \lambda_e'=\frac{\alpha}{\pi}\left[\ln\left(\frac{4\mathbf{k}'^2}{m^2}\right)-1\right]. \quad (58)$$

We can further assume that the third term of Eq. (52), although only broadly peaked at intermediate energies, contributes entirely to the final proton peak, yielding

$$\lambda_{p'}=\frac{\alpha}{\pi}\left[\frac{p'^0}{|\mathbf{p}'|}\ln\left(\frac{p'^0+|\mathbf{p}'|}{p'^0-|\mathbf{p}'|}\right)-2\right]. \quad (59)$$

Some bremsstrahlung strength still remains, due to the electron-proton interference term of Eq. (52) and to the nonpeaked contributions missed by the approximation of Eq. (57). This is true even in the ultrarelativistic limit, where one expects the peaking approximation to be the most valid (see Fig. 4). If one uses the closed form UR limit expressions of Eq. (37) to determine the difference $\delta_{\rm soft}(E_1)-\delta_{\rm soft}(E_2)$ between two energies, and compares this with the result using only the peaked strength described by Eqs. (58) and (59), one finds two missing terms. These are

$$\frac{\alpha}{\pi}\ln\left(\frac{E_2}{E_1}\right)4\ln\left(\frac{|\mathbf{k}|}{|\mathbf{k}'|}\right) \quad (60)$$

due to the electron-proton interference term $\delta_{\rm soft}^{ep}$, and

$$\Delta=\frac{\alpha}{\pi}\ln\left(\frac{E_2}{E_1}\right)2\ln\left(\frac{1-\cos(\theta_e)}{2}\right) \quad (61)$$

due to the nonpeaked strength in $\delta_{\rm soft}^{ee}$. In Table VIII we compare the exact calculation of the radiative correction factor in the UR limit [as given by Eq. (37)] with the factor generated in the peaking approximation. At all kinematics shown reasonable discrepancies show up, which can be understood by also tabulating the effects of removing the two missing terms. To resolve this our approach is to preserve the total strength (as evaluated in the UR limit) by distributing the contributions of these nonpeaked terms among the three photon peaks. We choose to split the two terms evenly between the electron peaks:

$$\tilde{\lambda}_e=\lambda_e+\frac{\alpha}{\pi}\left[2\ln\left(\frac{|\mathbf{k}|}{|\mathbf{k}'|}\right)+\ln\left(\frac{1-\cos(\theta_e)}{2}\right)\right],$$

$$\tilde{\lambda}_{e'}=\lambda_{e'}+\frac{\alpha}{\pi}\left[2\ln\left(\frac{|\mathbf{k}|}{|\mathbf{k}'|}\right)+\ln\left(\frac{1-\cos(\theta_e)}{2}\right)\right],$$

$$\tilde{\lambda}_{p'}=\lambda_{p'}. \quad (62)$$

This set of formulas can be termed the "extended peaking approximation" for single photon bremsstrahlung. To facilitate notations, we will use the notation λ below to mean $\tilde{\lambda}$, i.e., we will keep on assuming the "extended peaking approximation."

From Sec. III C, we know that including higher order bremsstrahlung is critical in evaluating the energy spectrum for low photon energies. One is then led to consider its effect on the angular distribution. Calculating such higher order contributions directly from Eq. (17) is a formidable task. Instead, we observe that the single photon peaking approximation,

$$\frac{d\sigma}{d\Omega_e d\omega}=\frac{d\sigma^{(1)}}{d\Omega_e}\bigg|_{ep}\frac{1}{\omega^0}(\lambda_e\delta(\hat{\omega}-\hat{k})+\lambda_{e'}\delta(\hat{\omega}-\hat{k}')+\lambda_{p'}\delta(\hat{\omega}-\hat{p}')), \quad (63)$$

effectively provides us with three independent single photon energy distributions, each for radiation in a fixed direction. We can then proceed in the manner of Sec. III C and determine a multiphoton spectrum, this time in terms of *three* energies: the total photon energies E_e, $E_{e'}$, and $E_{p'}$ emitted in each of the three peaked directions. The *total* radiated three-vector is then simply

$$\boldsymbol{\omega}_{\rm total}=E_e\hat{k}+E_{e'}\hat{k}'+E_{p'}\hat{p}'. \quad (64)$$

Furthermore, radiation *along* the direction of a given particle can be interpreted as radiation *due* to that particle. In this way we correct the q vector used to evaluate $d\sigma^{(1)}/d\Omega_e|_{ep}$ at the scattering vertex for energy radiated *before* the scattering (i.e., radiated by the incoming electron). This was seen in Sec. III A to be the source of the largest discrepancy between the soft photon approximation and full calculation for single photon radiation.

By analogy with Eq. (46), we obtain the cross section to all orders for radiating a total energy E_e along $\mathbf{k}$, $E_{e'}$ along $\mathbf{k}'$, and $E_{p'}$ along $\mathbf{p}'$, as well as any number of soft photons with energy less than ΔE_m:

$$\frac{d\sigma}{d\Omega dE_e dE_{e'} dE_{p'}}(\Delta E_m)=\frac{d\sigma^{(1)}}{d\Omega_e}\bigg|_{ep} e^{-\delta_{\rm soft}}(1-\delta_{\rm hard})\sum_{l=0}^{\infty}\sum_{m=0}^{\infty}\sum_{n=0}^{\infty}\frac{1}{l!}\left(\prod_{i=1}^{l}\int_{\Delta E_m}^{E_e} d\omega^{e0}_i\frac{\lambda}{\omega^{e0}_i}\right)\delta(\omega^{e0}_1+\cdots+\omega^{e0}_l-E_e)$$
$$\times\frac{1}{m!}\left(\prod_{i=1}^{m}\int_{\Delta E_m}^{E_{e'}} d\omega^{e'0}_i\frac{\lambda}{\omega^{e'0}_i}\right)\delta(\omega^{e'0}_1+\cdots+\omega^{e'0}_m-E_{e'})\frac{1}{n!}\left(\prod_{i=1}^{n}\int_{\Delta E_m}^{E_{p'}} d\omega^{p'0}_i\frac{\lambda}{\omega^{p'0}_i}\right)$$
$$\times\delta(\omega^{p'0}_1+\cdots+\omega^{p'0}_n-E_{p'}). \tag{65}$$

Using the same technique as in determining Eq. (48), one obtains

$$\frac{d\sigma}{d\Omega_e dE_e dE_{e'} dE_{p'}}$$
$$=\frac{d\sigma^{(1)}}{d\Omega_e}\bigg|_{ep} e^{-\delta_{\rm soft}(\Delta E_m)}(1-\delta_{\rm hard})e^{\lambda_e\ln(E_e/\Delta E_m)}\frac{\lambda_e}{E_e}F(\lambda_e)e^{\lambda_{e'}\ln(E_{e'}/\Delta E_m)}\frac{\lambda_{e'}}{E_{e'}}F(\lambda_{e'})e^{\lambda_{p'}\ln(E_{p'}/\Delta E_m)}\frac{\lambda_{p'}}{E_{p'}}F(\lambda_{p'}). \tag{66}$$

Again, the λ's are of order α, and so $F(\lambda_i)$ [Eq. (49)] is 1 to within a correction of order α^2. We see that the $1/\ln(\Delta E_m)$ dependence of $\delta_{\rm soft}(\Delta E_m)$ will be canceled by the other terms of the expression, taking care of the $\Delta E_m\to 0$ divergence of the single photon spectrum. By construction, the $\tilde{\lambda}$'s of the extended peaking approximation provide a subdivision of the terms of $\delta_{\rm soft}(\Delta E_m)$ which depend on ΔE_m:

$$\delta_{\rm soft}(E_1)-\delta_{\rm soft}(E_2)=\ln\left(\frac{E_2}{E_1}\right)(\tilde{\lambda}_e+\tilde{\lambda}_{e'}+\tilde{\lambda}_{p'}), \tag{67}$$

where E_1 and E_2 are two energies (note that this is true only in the UR limit). However, $\delta_{\rm soft}$ contains additional terms. Using Eq. (37), we find that these terms can also be subdivided in terms of the λ's:

$$\delta_e(\Delta E_m)=\lambda_e\ln\left(\frac{\sqrt{\epsilon\epsilon'}}{\Delta E_m}\right),$$
$$\delta_{e'}(\Delta E_m)=\lambda_{e'}\ln\left(\frac{\sqrt{\epsilon k'^0}}{\Delta E_m}\right),$$
$$\delta_{p'}(\Delta E_m)=\lambda_{p'}\ln\left(\frac{\sqrt{Mp'^0}}{\Delta E_m}\right). \tag{68}$$

Employing these definitions, we can take the limit $\Delta E_m\to 0$ to produce our final result for the multiphoton peaking approximation:

$$\frac{d\sigma}{d\Omega_e dE_e dE_{e'} dE_{p'}}=\frac{d\sigma^{(1)}}{d\Omega_e}\bigg|_{ep}(1-\delta_{\rm hard})e^{-\delta_e(E_e)}(-\delta_{e'}(E_e))e^{-\delta_{e'}(E_{e'})}(-\delta'_{e'}(E_{e'}))e^{-\delta_{p'}(E_{p'})}(-\delta'_{p'}(E_{p'}))$$
$$=\frac{d\sigma^{(1)}}{d\Omega_e}_{ep}(1-\delta_{\rm hard})\frac{\lambda_e\lambda_{e'}\lambda_{p'}}{(\sqrt{kk'})^{\lambda_e}(\sqrt{kk'})^{\lambda_{e'}}(\sqrt{Mp^{0'}})^{\lambda_{p'}}}\frac{1}{E_e^{1-\lambda^e}E_{e'}^{1-\lambda^{e'}}E_{p'}^{1-\lambda^{p'}}}. \tag{69}$$

The cross section thus factorizes neatly into three independent functions, for the total energy emitted in each of the three radiative tails.

The angular distribution implied by the above equation can be evaluated easily by a Monte Carlo program by randomly generating the energies emitted in each direction and adjusting the fermion vectors accordingly. However, it is worth studying the multiphoton angular distribution analytically, to determine the approximate shape of the multiphoton peaks. For our calculation to be valid (or useful), we must confirm that these peaks are substantially broader than the single photon peaks, which were approximated as delta functions in Eq. (51). To accomplish this, we employ a change of variables: from E_e, $E_{e'}$, and $E_{p'}$ to E, u, and v. Here, E is the total radiated energy $E_e+E_{e'}+E_{p'}$, while the emission direction is fixed by u and v:

$$u=\frac{E_e}{E_{e'}},$$

$$v=\frac{E_e}{E_{p'}}. \tag{70}$$

Note that u and v vary from 0 to ∞ with $u,v\to\infty$ corresponding to emission in the e direction, $u\to 0$ corresponding to emission in the e' direction, and $v\to 0$ corresponding to emission in the p' direction. The Jacobian between these two sets of variables is straightforward:

$$\frac{dE_e dE_{e'} dE_{p'}}{E_e E_{e'} E_{p'}}=\frac{dE du dv}{Euv}. \tag{71}$$

Consequently, the multiphoton emission cross section [Eq. (69)] can be rewritten easily in terms of the new variables. The dependence on the total energy E factorizes completely from the angular distribution, and the integration over emission angles can be accomplished, yielding

$$\frac{d\sigma}{d\Omega_e dE}$$

$$=\frac{d\sigma^{(1)}}{d\Omega_e}\bigg|_{ep}(1-\delta_{\rm hard})\frac{1}{(\sqrt{kk'})^{\lambda_e}(\sqrt{kk'})^{\lambda_{e'}}(\sqrt{Mp^{0'}})^{\lambda_{p'}}}$$

$$\times\frac{1}{E^{1-\lambda_e-\lambda_{e'}-\lambda_{p'}}}\times(\lambda_e+\lambda_{e'}+\lambda_{p'})$$

$$\times\frac{\Gamma(1+\lambda_e)\Gamma(1+\lambda_{e'})\Gamma(1+\lambda_{p'})}{\Gamma(1+\lambda_e+\lambda_{e'}+\lambda_{p'})}. \tag{72}$$

Recalling that the λ's are of order α, one finds that the ratio of gamma functions on the last line is 1 to within the usual $\mathcal{O}(\alpha^2)$ correction. To within this accuracy, this distribution agrees with the previous multiphoton formula, Eq. (48).

The analysis of the photon distribution simplifies greatly if one neglects proton radiation. Taking, in the peaking approximation, θ to be the angle between the photon and $\mathbf{k}$, and $\theta_{e'}$ to be the usual scattering angle between $\mathbf{k}$ and $\mathbf{k}'$ (note that in the peaking approximation the photon is emitted in the plane defined by $\mathbf{k}$ and $\mathbf{k}'$), one finds for $\theta\ll 1$

$$\frac{d\sigma}{d\Omega_e dE d\theta}\sim\frac{\sin(\theta_{e'})^{-\lambda_{e'}}}{\theta^{1-\lambda_{e'}}}, \tag{73}$$

and for $\theta-\theta_{e'}\ll 1$,

$$\frac{d\sigma}{d\Omega_e dE d\theta}\sim\frac{\sin(\theta_{e'})^{-\lambda_e}}{(\theta-\theta_{e'})^{1-\lambda_e}}. \tag{74}$$

The photon spectrum thus drops away from the peaks at the rate $\sim 1/\theta$. As this is more gradual than the $\sim 1/\theta^2$ falloff of the single photon peaks, our calculation of the multiphoton distribution from perfectly peaked single photons is reasonable. To quantify the effect of multiphoton emission on the angular distribution, Table IX shows the fraction of photons emitted at an angle greater than $\Delta\theta$ from either the initial or final electron directions for both the exact single-photon emission cross section and the multiphoton emission cross section, as calculated in the peaking approximation. For $\Delta\theta\sim 1°$, typically around 10% of the photons emitted in the multiphoton peaking approximation are in the intermediate region. This number increases slowly with Q^2. In contrast, the single-photon emission distribution gives about 3% in the intermediate region at $Q^2=1$ $(\mathrm{GeV}/c)^2$ and this number decreases rapidly with Q^2. Thus the multiphoton angular distribution does dominate the single-photon distribution in the intermediate region and as long as one is not probing the angular distribution of the photons on scales less then $\sim 1°$ it is consistent to calculate the angular distribution using the multiphoton peaking approximation.

TABLE IX. Effect of multiphoton emission on the angular distribution of emitted radiation. The fraction of photons emitted at angles larger than a cutoff value $\Delta\theta$ from either the initial or final electron direction are given for both single-photon emission and multiphoton emission.

Q^2 $(\mathrm{GeV}/c)^2$	$\Delta\theta$ (deg)	frac$^{1\gamma}$	frac$^{n\gamma}$
1	0.1	0.22	0.18
	1.0	0.03	0.11
	2.0	0.01	0.09
7	0.1	0.11	0.22
	1.0	0.01	0.14
	2.0	0.01	0.12
15	0.1	0.023	0.25
	1.0	0.003	0.18
	2.0	0.001	0.10

Of course, in the case of proton radiation, the peaking approximation is suspect from the very beginning. Its use hinges on the relatively small bremsstrahlung contribution of the proton, and on the resolution of the experiment. Also, as pointed out at the beginning of this section, at sufficiently high photon energies all radiative tails converge on the same $\tilde{E}_m=\tilde{p}_m$ kinematic path. The sensitivity to the precise angular distribution is thus most apparent at low photon energies. The effect of the peaking approximation will be examined in Sec. V for one of the NE18 kinematics.

B. Inclusion of external bremsstrahlung

External bremsstrahlung refers to the spectrum for the emission of bremsstrahlung photons in the field of nuclei *other* than the one participating in the hard scattering. The more massive outgoing proton is subject to much smaller accelerations, and emits a negligible amount of external radiation. On the other hand, the electrons will experience these losses as they move through the target material and traverse vacuum chamber windows and air gaps. External

bremsstrahlung can be treated essentially exactly, as has been shown, e.g., in [9,10]. In the remainder of this section we discuss how to add external bremsstrahlung in a consistent manner to our previous peaking approximations.

A numerical solution, in the complete screening approximation, for the probability that an electron of momentum $|k|$ radiates a total energy of $E^{\rm ext}$ when traversing t radiation lengths of material has been given by Early [16]. We will use the following analytic form for this probability distribution [9]

$$\frac{1}{\Gamma(1+bt)}\frac{bt}{E^{\rm ext}}\left(\frac{E^{\rm ext}}{|k|}\right)^{bt}\Phi^{\rm ext}\left(\frac{E^{\rm ext}}{|k|}\right), \tag{75}$$

where the parameter b depends on the atomic charge Z of the target material:

$$b=\frac{1}{9}\left(12+\frac{Z+1}{ZL_1+L_2}\right),$$

$$L_1=\ln(184.15)-\frac{1}{3}\ln(Z),$$

$$L_2=\ln(1194)-\frac{2}{3}\ln(Z). \tag{76}$$

The function $\Phi^{\rm ext}$ is a correction for large photon energies, expanded to second order in $E^{\rm ext}/|k|$:

$$\Phi^{\rm ext}(x)=1-x+\frac{3}{4}x^2. \tag{77}$$

This analytic form differs from the numerical solution by a fraction that varies between about $t/10$ and $t/5$ as E^{ext} varies between 0 and 0.8ϵ for $t<0.1$ [16]. For example, the deviation at $E^{\rm ext}\simeq 0$ is $\sim 1\%$ for a $t=10\%$ radiator. The discrepancy increases for $E^{\rm ext}>0.8\epsilon$, but this is typically outside the experimental acceptances.

External radiation is far simpler to treat than internal. First of all, the particles radiate independently and so incoherently, and this eliminates the nonpeaked strength caused by the interference terms of internal bremsstrahlung. Furthermore, proton radiation is suppressed relative to electron radiation by the factor $(m/M)^2<10^{-6}$, and so can be neglected entirely. Equation (69) can thus be extended in a straightforward way to include the contributions from external radiation along the $\mathbf{k}$ and $\mathbf{k}'$ directions:

$$\frac{d\sigma}{d\Omega_e dE_i^{\rm int}dE_i^{\rm ext}dE_f^{\rm int}dE_f^{\rm ext}}=\left.\frac{d\sigma^{(1)}}{d\Omega_e}\right|_{ep}(1-\delta_{hard})\frac{1}{\Gamma(1+bt_i)}\frac{bt_i}{E_i^{\rm ext}}\left(\frac{E_i^{\rm ext}}{|k|}\right)^{bt_i}$$
$$\times\frac{\lambda_i}{E_i^{\rm int}}\left(\frac{E_i^{\rm int}}{\sqrt{|kk'|}}\right)^{\lambda_i}\frac{1}{\Gamma(1+bt_f)}\frac{bt_f}{E_f^{\rm ext}}\left(\frac{E_f^{\rm ext}}{|k'|}\right)^{bt_f}\frac{\lambda_f}{E_f^{\rm int}}\left(\frac{E_f^{\rm int}}{\sqrt{|kk'|}}\right)^{\lambda_f}. \tag{78}$$

Here, the internal proton contribution has been omitted for convenience, and the subscripts i and f have been introduced to indicate the initial and final electron arms. Equation (78), when taking into account the internal proton contributions following Eq. (69), represents the result of adding internal and external bremsstrahlung in a consistent fashion, and is the final result of a generalized peaking approximation. Since both $E_i^{\rm int}$ and $E_i^{\rm ext}$ are emitted in the same direction, we can again rewrite the distribution in terms of the total energies E_i and E_f radiated along $\mathbf{k}$ and $\mathbf{k}'$. This problem is exactly analogous to the transformation made between Eqs. (69) and (72), where a change of variables was made from three energies E_e, $E_{e'}$, $E_{p'}$ to a total energy E and angle variables u and v. The result is

$$\frac{d\sigma}{d\Omega_e dE_i dE_f}=\left.\frac{d\sigma^{(1)}}{d\Omega_e}\right|_{ep}(1-\delta_{hard})\frac{1}{\Gamma(1+bt_i)}\frac{1}{\Gamma(1+bt_f)}$$
$$\times\frac{(bt_i+\lambda_i)}{k^{bt_i}(\sqrt{kk'})^{\lambda_i}}\frac{(bt_f+\lambda_f)}{k'^{bt_f}(\sqrt{kk'})^{\lambda_f}}$$
$$\times\frac{1}{E_i^{1-\lambda_i-bt_i}}\frac{1}{E_f^{1-\lambda_f-bt_f}}. \tag{79}$$

We thus see that the λ's of internal radiation play much the same role as the material thickness bt of external bremsstrahlung. One can also express the external radiation contribution in terms of the usual bremsstrahlung functions δ_{soft}. One obtains forms which are very similar to those of Eq. (68):

$$\delta_e^{\rm ext}(\Delta E_m)=bt_i\ln\left(\frac{k}{\Delta E_m}\right),$$

$$\delta_{e'}^{\rm ext}(\Delta E_m)=bt_f\ln\left(\frac{k'}{\Delta E_m}\right). \tag{80}$$

These functions can simply be added to the corresponding $\delta(\Delta E_m)$ values for internal radiation in Eq. (69), yielding the same result as Eq. (79).

Thus far, the correction function $\Phi^{\rm ext}(E^{\rm ext}/|k|)$ has been neglected. At NE18 kinematics, the ratio $E_\gamma/|k|$ in which the function is expanded is small ($\leqslant 0.1$). Consequently we take only the first order term of $\Phi^{\rm ext}(x)$ of Equation 77 and include it in Eq. (78). Carrying through the angular integration, one obtains multiplicative factors $\bar{\Phi}_i^{\rm ext}$ and $\bar{\Phi}_f^{\rm ext}$ to include in Eq. (79):

$$\overline{\Phi}_i^{\rm ext}\left(\frac{E_i}{|k_i|}\right)=1-\frac{bt_i}{bt_i+\lambda_i}\frac{E_i}{|k_i|}. \tag{81}$$

(The same form applies for $\overline{\Phi}_f^{\rm ext}$ with $i\rightarrow f$ everywhere.)

V. EXPERIMENTAL SIMULATIONS

This section describes two independent Monte Carlo programs used to simulate the NE18 experiment. Radiative effects are simulated using three separate methods, each involving different approximations. The three methods, two described in Sec. V A and one in Sec. V C, are found to produce consistent results.

A. Description of the experimental simulation

A Monte Carlo program, named SIMULATE [17], randomly generated the momenta and angles of the scattered electron and proton vectors (i.e., the 6 quantities in terms of which the differential cross section is defined) with a flat distribution over limits calculated to exceed the experimental acceptance. The energy and position of the incident electron at the target were also generated randomly, to match the energy and spatial spread of the beam, and the beam energy was corrected for ionization losses in the target. With a basic event at the scattering vertex now determined, the possibility that any or all of the particles emitted real or virtual photons was modeled and the particle vectors were adjusted accordingly. The scattered electron and proton vectors were then transported through the target, applying ionization losses and a multiple scattering distribution, and subsequently transported through the spectrometers. Monte Carlo models of the optics, apertures, and interfering materials of the spectrometers were employed. Both forward and backward sets of matrix elements were used, to simulate the optical resolution of the magnetic systems. Once the particle vectors were reconstructed back to target, they were corrected to the scattering vertex using the same mean energy loss calculations employed in the actual data analysis, and E_m and p_m were determined [17,18]. The successful events were stored in histograms, with each event being assigned a weight of $K\sigma_{ep}S[1/(1-\delta_{\rm hard})]W_{gen}$. In the case of the $A(e,e'p)$ reaction K equals a kinematic factor, S represents the spectral function or the probability to find a proton with certain missing momentum and certain binding energy inside the target nucleus A, and σ_{ep} is the electron-proton cross section corrected for off-shell effects according to the prescription of DeForest [12]. Note that this is the form encountered in the plane-wave impulse approximation (PWIA) description of $A(e,e'p)$ reactions. In the case of the $^1{\rm H}(e,e'p)$ reaction K equals unity, S equals a delta function, and σ_{ep} is the standard electron-proton scattering cross section. The factor $(1-\delta_{\rm hard})^{-1}$ is the correction for radiative diagrams involving hard virtual photons. The ''generation weight'' (W_{gen}) comes from the following source. To increase computer speed, the limits in which event quantities are generated can be refined once partial information about an event is known. These refinements are based on the acceptance limits of the spectrometers, the cuts imposed on reconstructed E_m, p_m, and particle vectors, and the range in E_m (at the vertex) over which the spectral function is defined. These refined limits are especially important in the generation of radiation. For example, to take into account the possibility that a scattered electron ''radiated into'' the spectrometer momentum acceptance from a higher momentum, one must use generation limits in momentum which are much wider than the acceptance. However, once the electron's momentum has been generated, one can determine the range of photon energy required to produce a successful event. The generation weight reduces the event weight to compensate for the restricted limits employed. Finally, the results histograms were normalized so that the number of events in each bin would correspond to the number of counts expected from the experiment. The results were thus multiplied by $\mathcal{L}(\Delta\epsilon'\Delta\Omega_{e'}\Delta\epsilon'\Delta\Omega_{p'})_{gen}/N_{gen}$ where $\mathcal{L}$ is the experimental luminosity, and the other terms refer to the phase space volume and total number of events used by the generation. Each histogram bin was assigned an inverse fractional error equal to the square root of the total Monte Carlo weight contributing to the bin.

Two models of the radiative effects are included in the Monte Carlo program SIMULATE. (A third method for including radiative effects, also included in the Monte Carlo program, is described in Sec. V C.) The first uses the multiphoton energy distribution of Eq. (48), evaluated using the full SPA expressions of Eqs. (32) and (33). The angular distribution is taken to be the pure peaking approximation of Eq. (51). The strength is distributed among the three tails $i=1,2,3$ using the fractions $\lambda_i/\Sigma_i\lambda_i$ (i is shorthand for the usual tail subscripts e, e', p'). The second method tries instead to obtain the correct multiphoton angular distribution by generating the total photon energies E_e, $E_{e'}$, $E_{p'}$ emitted along each direction, and summing the resulting photon vectors according to Eq. (64). The distributions are generated according to the independent forms found for each tail in Eq. (69). These energy distributions were calculated using the approximate closed form expressions of Eq. (37), found in the ultrarelativistic limit of high momentum transfer and particle momenta. These two choices represent a tradeoff between the best available forms for the photon energy (first technique) and angular (second technique) distributions. The first method can thus be referred to as the ''peaking'' technique, and the second as the ''multiphoton'' technique. Note that these names are somewhat misleading: the ''peaking'' formalism certainly involves contributions from bremsstrahlung radiation to all orders, and the ''multiphoton'' prescription involves the peaking approximation at the one photon level. One hopes, of course, that the two prescriptions give very similar results and this indeed turns out to be the case. The distributions of counts calculated by SIMULATE using the two techniques are sufficiently similar that one is hard pressed to see any differences on a plot of the projections in E_m and p_m. The integrated yields are less than 1% different at all Q^2. This excellent agreement indicates the lack of sensitivity of our results to the fine details of the photon angular distribution, and the validity of the UR limit at the energies we consider.

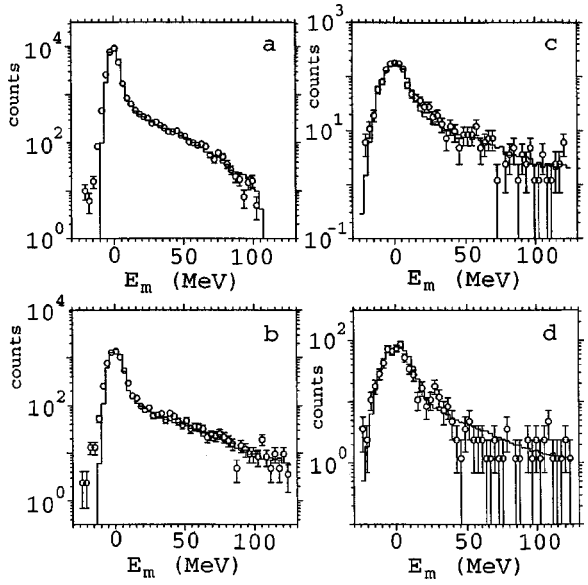

FIG. 5. Distribution in E_m of coincidence events recorded for the hydrogen target, compared with the prediction of the Monte Carlo program SIMULATE, for $Q^2=1$ (a), 3 (b), 5 (c), and 6.8 (d) $(\mathrm{GeV}/c)^2$, respectively.

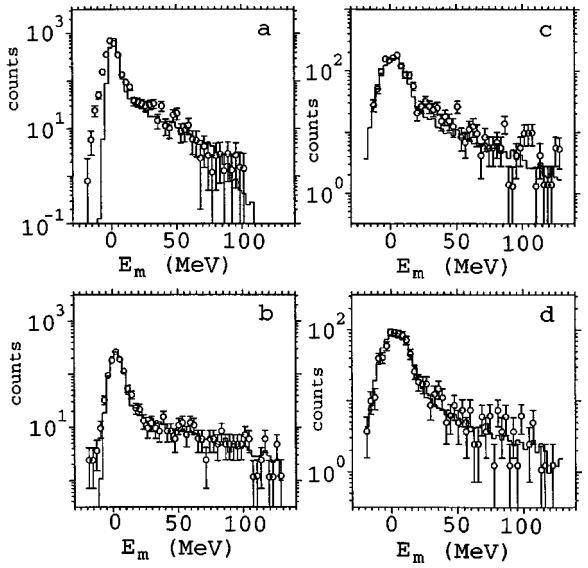

FIG. 6. Distribution in E_m of coincidence events recorded for the deuterium target, compared with the prediction of the Monte Carlo program SIMULATE, for $Q^2=1.2$ (a), 3 (b), 5 (c), and 6.8 (d) $(\mathrm{GeV}/c)^2$, respectively.

B. Comparison with experimental results

The distribution of hydrogen data *counts* in E_m and p_m compared with the Monte Carlo calculation provides a precise test of many aspects of the calculation. The true distribution of elastic events is precisely localized at $E_m=0$ and $\mathbf{p_m}=0$; any deviation from this must be due to the improper understanding of kinematics, deviations from the mean energy loss corrections, experimental resolution, and particle radiation. The last two effects should be correctly modeled by the Monte Carlo. In particular, a comparison of the data and Monte Carlo on the hydrogen radiative tail provides a precise test of the radiative procedure, unclouded by other physics. Finally the $^1\mathrm{H}(e,e')$ data (corrected for possible proton absorption losses in the target, spectrometer, and detector materials) must be consistent with previous $^1\mathrm{H}(e,e')$ data.

The distribution of $^1\mathrm{H}(e,e'p)$ data counts as a function of E_m is presented for the four values of Q^2 in Fig. 5. Superimposed on these figures is the corresponding Monte Carlo calculation. In this Monte Carlo simulation we used the dipole form factor for the proton electric form factor and the parametrization of Gari and Krümpelmann for the proton magnetic form factor [19,14]. Also included here are the E_m distributions for $^2\mathrm{H}(e,e'p)$ (Fig. 6), as the single deuterium bound state is very sharply peaked at the binding energy of 2.2 MeV and so ^{2}H data in this coordinate provide the same precise test of the radiative procedure as ^{1}H. Here we used the off-shell prescription used by DeForest [12] to account for the electron-proton scattering cross section of the bound proton, and the Bonn nucleon-nucleon potential [20] to account for the proton momentum distribution in the ^{2}H target nucleus (see also Ref. [21]). Note that all the calculations include the contribution from the recoiling proton in applying the radiative corrections. The figures clearly demonstrate that the radiative prescription describes the data to within its statistical uncertainty. As a quantitative measure of the E_m and p_m dependent agreement one can evaluate the ratio of the hydrogen experimental data to the hydrogen Monte Carlo data with a variety of E_m cuts. One finds that this ratio varies by an amount well within the statistical error of the data for upper E_m cutoffs from 50 to 130 MeV. The statistics provide a precision from 1% at $Q^2=1$ $(\mathrm{GeV}/c)^2$ to 4% at $Q^2=7$ $(\mathrm{GeV}/c)^2$.

The angular distribution of the emitted photons can be reconstructed from the measured $\mathbf{p_m}$ [22]. We will here consider the $Q^2=1$ $(\mathrm{GeV}/c)^2$ case and only consider events with a missing energy ($\simeq\omega^0$) larger than 30 MeV since in the region $\omega^0\rightarrow 0$ MeV the experimental resolutions, 8 MeV (10 MeV/c) in missing energy (momentum), do not permit an accurate reconstruction of the photon angle. Fig. 7 shows the angular distribution of the count rate for events with $E_m>30$ MeV. It is seen that electron radiation is predominantly in the direction of the initial and final electrons, in accordance with the peaking approximation [23]. Note that a broad distribution of events is seen in the direction of the outgoing proton. Next, the angular distributions were calculated in the soft-photon limit. In this case the proton contribution corresponds to radiation from a Dirac particle with the usual form factors $F_1(Q^2)$ and $F_2(Q^2)$. The differential cross section was reduced to the cross section for (multi-) photon emission with total energy ω and angle ϑ_ω in the scattering plane. For this we used polar coordinates, integrating over the range of $\tan(\phi_\gamma)$ accepted by the phase space. Effects arising from imperfect knowledge of the phase space were suppressed through an energy cut, $\omega^0<80$ MeV, applied for radiated photons along the incident electron beam. No normalization factors were used. As Fig. 7 shows, the agreement between data and simulation is excellent (note that only about 3×10^3 out of a total of 5×10^4 events have

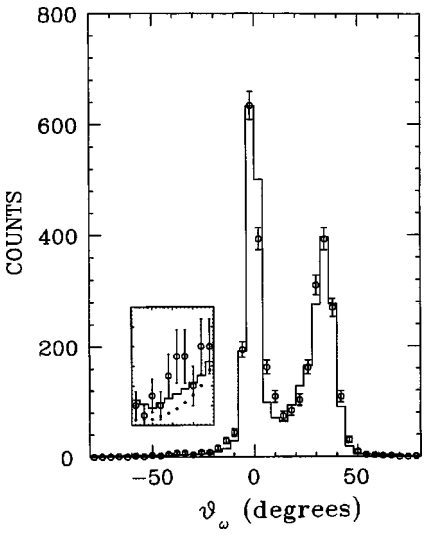

FIG. 7. Calculated angular distribution of radiated events in comparison with NE18 data for $\omega^0>30$ MeV [22]. The solid (dotted; see inset) curve shows the prediction in the soft-photon limit of the Monte Carlo program SIMULATE for electron and proton contributions (electron only). The central angle ϑ_ω for the incident (scattered) electron and outgoing proton are $0°$ ($37.3°$) and $-43.3°$, respectively. Note that the inset shows the region $-60°<\vartheta_\omega<-20°$ with a different vertical scale.

radiated more than 30 MeV). To enhance the sensitivity to the proton contributions to the radiative corrections, we have highlighted in the inset of Fig. 7 the region sensitive to these proton contributions. That such a region exists was illustrated before in Fig. 4. One can argue that a better description is obtained including both proton and electron contributions (solid curve in inset) [22].

We would like to emphasize the differences between Figs. 4 and 7. In Fig. 4 the prominent dip along the proton angle reflects the character of dipole radiation boosted along the particle's momentum, emphasized in the single-photon limit. The electron radiation peaks also have sharp minima at their maxima, but because the boost of the dipole pattern is so large, the minima are so narrow that they are not visible. In Figure 7 a complete angular distribution of radiated photons is calculated, where *all* multiphoton contributions are taken into account.

C. Modified equivalent radiator method

In Sec. IV A we determined values for λ_e, $\lambda_{e'}$, and λ_p by integrating the various terms of the photon angular distribution $A(\hat{\omega})$ and distributing the results among the three particle directions. This can be arbitrary, e.g., we decide to split the contributions from Eqs. (60) and (61) evenly amongst the electron and scattered electron direction.

Alternatively, for thin targets ($bt<0.1$) in inclusive electron scattering it has been shown [9] that the full effect of bremsstrahlung can be simply approximated by dividing the target in two equivalent-length radiators. This is termed the equivalent radiator approximation. In this section we will give a generalization of this approximation for the $A(e,e'p)$ reaction, termed the ''modified equivalent radiator method'' (MERM) [18]. In this method we choose the distribution amongst the various λ's, again termed λ_e, $\lambda_{e'}$, and λ_p, different than in Sec. IV A: two constraints are given by the *theoretical* energy dependence (i.e., integrated over the photon angular distribution) of the radiated events in energy transfer and in missing energy. A third constraint we will impose.

TABLE X. Comparison of the equivalent radiator thicknesses λ for various kinematics. Values λ^{EQ} are from Eq. (82), λ are from Eqs. (58) and (59), and λ^{mod} are from Eqs. (86)–(90).

Q^2 $(\mathrm{GeV}/c)^2$	λ^{EQ} (%)	λ_e (%)	$\lambda_{e'}$ (%)	$\lambda_{p'}$ (%)	λ_e^{mod} (%)	$\lambda_{e'}^{mod}$ (%)	$\lambda_{p'}^{mod}$ (%)
1	3.322	3.936	3.767	0.042	3.502	3.614	0.037
3	3.561	4.149	3.790	0.326	3.652	4.282	0.287
5	3.669	4.279	3.790	0.485	3.786	4.619	0.429
7	3.736	4.369	3.790	0.590	3.883	4.836	0.524

Based upon the similarity of Eqs. (68) and (80), the standard equivalent radiator approximation simulates internal bremsstrahlung by passing the incident and scattered electron through two effective external radiators, both with $bt=\lambda^{EQ}$:

$$\lambda^{EQ}=\frac{\alpha}{\pi}\left[\ln\left(\frac{Q^2}{m^2}\right)-1\right]. \tag{82}$$

Note that for internal bremsstrahlung b and t are separately meaningless. The value is typically $\lambda^{EQ}\sim 3.5\%$ (see Table X). The equivalent radiator method assumes the angle peaking approximation, where the radiation changes the magnitude but not the direction of the electron's momentum. Similarly, Borie and Drechsel [24] included internal bremsstrahlung assuming such peaking approximation, using the cross sections for first-order photon emission. Results using this method do not differ distinctly from the equivalent radiator approximation.

The modified equivalent radiator method relies on a similar technique to simulate the effects of internal radiation on the count rates and kinematics of an $A(e,e'p)$ reaction. The modification is necessary to reproduce both the exact energy loss ($\nu=\epsilon-\epsilon'$) dependence due to radiation, as given by Eq. II.6 of Ref. [6], and the exact missing energy dependence due to radiation, given by Eqs. (32) and (33). This is important because events are *simultaneously* subject to the $\Delta\epsilon'$ range given by the electron arm momentum acceptance and the ΔE_m range applied in the coincidence analysis. (Here $\Delta\epsilon'=\epsilon'_{el}-\epsilon'$ and $\Delta E_m=E_m^{el}-E_m$ are the radiation-induced reductions in the energies ϵ' and E_m from their elastic values.) The MERM differs from the standard equivalent radiator approximation in two ways. First, as the scattering energy increases, a few percent of the radiation becomes peaked near the scattered proton direction (the large acceleration of the proton in the scattering begins to overcome the suppression of radiation by its high mass). Thus, the scattered proton is also passed through an equivalent external radiator, with bt values between 0.00037 [at $Q^2=1$ $(\mathrm{GeV}/c)^2$] and 0.00524 [$Q^2=7$ $(\mathrm{GeV}/c)^2$] (see Table X). Second, the

three equivalent radiators have three different thicknesses (the equality of the incoming and outgoing electron radiators in the standard equivalent radiator approximation is only valid in the limit of no target recoil). The thicknesses are adjusted to reproduce the theoretical radiation tail distribution of the $^1H(e,e'p)$ reaction simultaneously as functions of the scattered electron energy ϵ' and the missing energy E_m. It is convenient to determine the necessary thicknesses in the limit $\Delta\epsilon'$, $\Delta E_m \ll \epsilon, \epsilon'$; validity at higher $\Delta\epsilon'$ and ΔE_m is discussed below. Referring to Eq. (22), we observe that Eq. (32) has a logarithmic dependence on ΔE_m: $\delta_{\rm soft}(\Delta E_m) = \lambda_{E_m} \ln(\Delta E_m) + \ln N_{E_m}$. For elastic kinematics in the soft photon approximation, λ_{E_m} and N_{E_m} are functions of ϵ and $\theta_{e'}$ only. Thus the E_m dependence of the tail as given by Eq. (40) is

$$e^{-\delta_{soft}(E_m)} = N_{E_m} (\Delta E_m)^{\lambda_{E_m}}. \tag{83}$$

Inspection of Eq. II.6 of Ref. [6] immediately yields analogous functional forms for $\delta_{soft}(\Delta\epsilon')$ and $e^{-\delta_{soft}(\Delta\epsilon')}$:

$$e^{-\delta_{soft}(\Delta\epsilon')} = N_{\epsilon'} (\Delta\epsilon')^{\lambda_{\epsilon'}}. \tag{84}$$

As discussed in the last part of Sec. III B, the only difference between $\delta_{soft}(E_m)$ and $\delta_{soft}(\Delta\epsilon')$ is a change in the integration region. Thus one finds the exponent $\lambda_{E_m} = \lambda_{\epsilon'} \equiv \lambda_{\rm tot}$ at all kinematics. This fact will allow simultaneous matching of both energy dependences. In practice $\lambda_{\rm tot}$ is determined numerically by evaluating Eq. (32) for two different values of E_m.

In the MERM, the internal radiation is simulated by passing the beam electron, scattered electron, and outgoing proton through external radiators with bt values λ_e, $\lambda_{e'}$, and $\lambda_{p'}$. Analytic expressions for the resulting ΔE_m and $\Delta\epsilon'$ dependences are used to choose λ values that reproduce the theoretical energy dependence of internal radiation [Eqs. (83) and (84)]. The expression for the $\Delta\epsilon'$ dependence induced by three external radiators, valid for small $\Delta\epsilon'$ [where $\Phi^{\rm ext}(x) \simeq 1$], is derived in Appendix F of Ref. [18]:

$$\frac{d\sigma}{d\Omega_e}(\epsilon' \geqslant \epsilon'_{el} - \Delta\epsilon') = \left.\frac{d\sigma^{(1)}}{d\Omega_e}\right|_{ep} \frac{1}{\Gamma(1+\lambda_e+\lambda_{e'}+\lambda_{p'})} \times \left(\frac{R_e \Delta\epsilon'}{\epsilon}\right)^{\lambda_e} \left(\frac{\Delta\epsilon'}{\epsilon'_{el}}\right)^{\lambda_{e'}} \left(\frac{R_p \Delta\epsilon'}{p'^0}\right)^{\lambda_{p'}}. \tag{85}$$

The recoil factor R_e (R_p) takes into account that radiation of energy ω by the beam electron (outgoing proton) changes ϵ' by a amount $R_e\omega$ ($R_p\omega$). Here $R_e < 1$ because the energy ω radiated by the beam electron comes from a reduction in ϵ' and in the kinetic energy of the recoil proton; for small photon energies $R_e \approx (\epsilon/\epsilon'_{el})^2$. The Monte Carlo using the MERM technique determines the amount of energy radiated by the proton before computing ϵ'; ϵ' is chosen so that the proton is left on shell after it emits the real photons. For small photon energies the resulting proton recoil correction $R_p \approx [M + 2\epsilon \sin^2(\theta_{e'}/2)]/(p'^0 - |p'|)$. The equation for $d\sigma(E_m \leqslant E_m^{el} + \Delta E_m)/d\Omega_e$ is obtained from Eq. (85) using the substitutions $\Delta\epsilon' \to \Delta E_m$ and $R_e, R_p \to 1$ [cf. Eq. (6)]. The resulting formula satisfies an important consistency check: for a trivial scattering process $[d\sigma^{(1)}/d\Omega_e = 1]$, it reduces to the integral of Eq. (75) over $E^{\rm ext}$ with $bt = \lambda_e + \lambda_{e'} + \lambda_{p'}$ and $E^{\rm ext} = \Delta E_m$ (assuming $\Phi^{\rm ext} \simeq 1$).

Choosing the λ parameters according to Eqs. (58) and (59), while an improvement over the standard equivalent radiator technique [Eq. (82)], still would not satisfy the theoretical ϵ' and E_m dependences of Eqs. (83) and (84). Such an approach would e.g., neglect the ''missing'' terms of Eqs. (60) and (61), and, indeed, using Eq. (62) instead of Eqs. (58) and (59) gives closer agreement. Instead, we require the modified equivalent radiator approximation to reproduce the theoretical values of $N_{\epsilon'}$, N_{E_m}, and $\lambda_{\rm tot}$. Conveniently, Eq. (85) exhibits the same $\Delta\epsilon'$ dependence as the theory $[\sim(\Delta\epsilon')^{\lambda_{\rm tot}}]$ for small $\Delta\epsilon'$, so long as the λ's used in the calculation are chosen so that

$$\lambda_e + \lambda_{e'} + \lambda_{p'} = \lambda_{\rm tot}. \tag{86}$$

Multiplication of the cross section by the proper normalization factor (representing, among other things, the contribution of the hard corrections) allows the calculation to agree with Eq. (84) at small $\Delta\epsilon'$. Because $\lambda_{E_m} = \lambda_{\epsilon'}$ $(= \lambda_{tot})$, the calculation can *simultaneously* satisfy Eqs. (83) and (84) at all small values of $\Delta\epsilon'$ and ΔE_m if it uses λ_e and $\lambda_{p'}$ that satisfy

$$R_e^{\lambda_e} R_p^{\lambda_{p'}} = \frac{N_{\epsilon'}}{N_{E_m}} = e^{\delta_{\epsilon'} - \delta_{E_m}}. \tag{87}$$

Reproducing the theoretical $N_{\epsilon'}$, N_{E_m}, and $\lambda_{\rm tot}$ places three conditions on the four unknowns (λ_e, $\lambda_{e'}$, $\lambda_{p'}$, and the normalization). The theoretical integral of the cross section over another observable (for instance p'^0) could provide a fourth condition ($N_{p'}$) and remove the remaining ambiguity. However, the calculation is insensitive at the $<0.5\%$ level to even a 50% change in the ratio of $\lambda_{p'}$ to λ_e. For definiteness, we choose the ratio $\lambda_{p'}/\lambda_e$ to be equal to $\lambda_{p'}^{peak}/\lambda_e^{peak}$ given by Eqs. (58) and (59):

$$\lambda_e = f_t \lambda_e^{peak}, \tag{88}$$

$$\lambda_{p'} = f_t \lambda_{p'}^{peak}, \tag{89}$$

where the fraction f_t varies between 0.88 and 0.89:

$$f_t = \frac{\delta_{\epsilon'} - \delta_{E_m}}{\ln(R_e^{\lambda_e^{peak}} R_p^{\lambda_{p'}^{peak}})}. \tag{90}$$

The λ values resulting from these prescriptions are listed as λ^{mod} in Table X. The equivalent radiator parameters are evaluated for central kinematics, and are not adjusted for the kinematics of each event. The errors produced by neglecting variations in E and $\theta_{e'}$ are negligible for the NE18 acceptan-

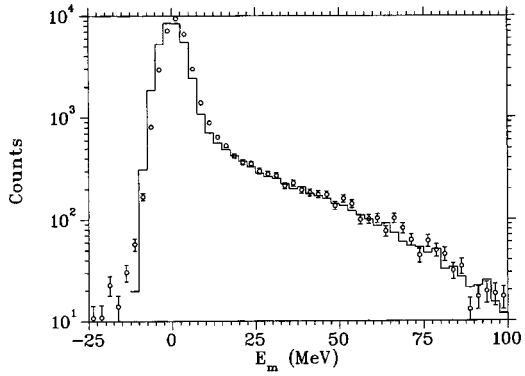

FIG. 8. E_m distribution of ^{1}H$(e,e'p)$ events at $Q^2=1$ $(\mathrm{GeV}/c)^2$. The data (points with error bars) are from the NE18 experiment [11] and the calculation (histogram) is performed with the modified equivalent radiator method.

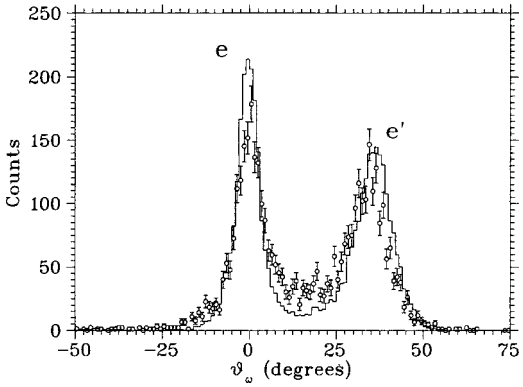

FIG. 9. Comparison between the ^{1}H$(e,e'p)$ data and the modified equivalent radiator Monte Carlo simulation for the angle $\vartheta_\omega=\tan^{-1}(P_{m,x}/P_{m,z})$ at $Q^2=1$ $(\mathrm{GeV}/c)^2$. Note that ϑ_ω is the projected angle of the radiation in the horizontal plane rather than the spherical coordinate ϑ_γ. To reduce the effects of the finite resolution, only events with $E_m>20$ MeV are displayed. The peaks from radiation directed along the incident beam and the scattered electron direction are clearly visible at $\vartheta_\omega=\theta_e=0$ and $\vartheta_\omega=\theta_{e'}=37.3°$.

ces [18] ($<0.04\%$ in the normalization and <0.0012 in the λ values). Due to approximations in the formulas for $\delta_{\epsilon'}$ and δ_{E_m}, Eqs. (84) and (83) are not valid for $\Delta\epsilon' \geqslant \epsilon'/(1+2\epsilon/M)$ [4]. The equations neglect two effects, which are actually present in the modified equivalent radiator technique: $d\sigma^{(1)}(E-R_e\Delta\epsilon')/d\Omega_e > d\sigma^{(1)}(E)/d\Omega_e$, and $\Phi^{\mathrm{ext}}(\omega/E)<1$. Thus, the modified equivalent radiator calculation maintains good agreement ($<0.5\%$) with exact calculations of the radiation even for large $\Delta\epsilon'$.

One might wonder why external radiation is able to exactly reproduce the energy dependence for internal radiation at small photon energies. The single-photon expressions for internal and external radiation have the same $1/\omega$ dependence. Agreement is maintained in the infinite-photon limit because the *coherent* multiple-photon exponentiation in Eq. (85) serves the same role as the *incoherent* multiple-collision factor $(E^{\mathrm{ext}})^{bt}$ in Eq. (75). To see this, recall Eqs. (83) and (84), $e^{\delta}=N\omega^{\lambda}$. The tail height (divided by the electron-proton scattering cross section) is $de^{\delta}/d\omega=N\lambda\omega^{\lambda-1}$. For $\lambda=bt$, this has the same energy (ω or E^{ext}) dependence as Eq. (75), the multicollision form for external radiation. Now consider the single-photon version of the above, found by taking the logarithm: $\delta=\lambda\ln\omega+\ln N$, with tail height $d\delta/d\omega=\lambda/\omega$. The single-photon form for external radiation is found in the $t\to 0$ limit of Eq. (75): bt/E^{ext} [taking $\Phi^{\mathrm{ext}}(E^{\mathrm{ext}}/|k|)\simeq 1$]. Thus the internal and external radiation have the same energy dependence in both the multi- and single-photon limits, and the conversion from the single-photon to the coherent multiple-photon form is mathematically identical to the conversion to the incoherent multiple-collision form.

Figure 8 demonstrates the success of the modified equivalent radiator technique in describing the distribution of the NE18 ^{1}H$(e,e'p)$ data counts as a function of E_m at a momentum transfer squared Q^2 of 1 $(\mathrm{GeV}/c)^2$ (see Table I). One can see that also in this method the falloff in count rate over three orders of magnitude is well described by the Monte Carlo simulation. The equivalent radiator procedure used in this Monte Carlo simulation implicitly makes two assumptions about the effect of internal bremsstrahlung on kinematics: (1) photons can be treated as being emitted exactly parallel to the outgoing particles (the angle peaking approximation), and (2) photons emitted along the incident electron, scattered electron, or scattered proton direction can be treated as if they were emitted by that particle, and thus cause a change in energy only for that particle (the latter assumption is especially relevant for the cross section weighting in Monte Carlo simulations). In Fig. 9 one finds that the modified equivalent radiator approximation does a good job of reproducing the observed widths of the peaks in the angular distribution of the photon events. To reduce the sensitivity to the finite resolutions, only events with $E_m>20$ MeV are displayed. The events at $\vartheta_\omega\approx 15°$ are the result of radiation by the electron both before and after the scattering. The incoherent addition of the radiation before and after the scattering in the equivalent radiator approximation underpredicts the strength given by the coherent interference of the corresponding radiative diagrams. However, the missing strength is less than 10% of the counts at $20\ \mathrm{MeV}/c<\omega<200\ \mathrm{MeV}/c$—that is, less than 1% of the total counts. In only a fraction of these events would the exact photon angle make the difference between the outgoing particles being inside or outside of the experimental acceptance, and thus the error is insignificant unless one is interested in a detailed and high-precision understanding of the angular distributions of radiated $(e,e'p)$ events.

The validity of assumption (2), that photons emitted *along* one of the particle directions can be treated as if emitted *by* that particle, is demonstrated by Fig. 10. Kinematics ensure that radiation along the scattered electron direction has $R=1$, and radiation in the incident beam direction has $R\approx R_e$. However, the resemblance of data and Monte Carlo simulation also supports the numerical procedure (of vertex cross section evaluation) we chose to calculate the effects of radiation. In the figure, the cross over from the $\vartheta_\omega<15°$ to $\vartheta_\omega>15°$ occurs at $R\approx 1.4$ for both data and Monte Carlo calculation. The calculation's underestimate of events at $\Theta\approx 15$ mr, discussed above, maps here to an underestimate at $R\approx 1.4$.

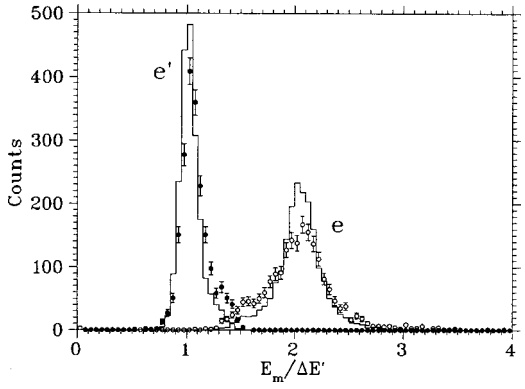

FIG. 10. Comparison between the ^{1}H$(e,e'p)$ data and the modified equivalent radiator Monte Carlo simulation for the recoil ratio $R=E_m/\Delta\epsilon'$ at $Q^2=1$ $(\mathrm{GeV}/c)^2$. To reduce the effects of the finite resolution, only events with $E_m>20$ MeV are displayed. The solid circles and left-hand histogram are the data points and Monte Carlo prediction for $\vartheta_\omega>15°$, corresponding to the peak at θ_e' in Fig. 9. Note these events have the ratio $R\approx R_{e'}=1$. The open circles and right-hand histogram are for the peak at $\theta_e=0$ $(\vartheta_\omega<15°)$, and have $R\approx R_e=2.07$.

The MERM is effectively very similar to the ''peaking'' technique described in Sec. V A, which uses the best available form for the photon energy. Both techniques reproduce the theoretical E_m dependence and provide a reasonable description of the angular distribution of the radiation by incorporating simultaneous radiation along the e, e', and p' directions. The MERM technique improves on the ''peaking'' technique by reproducing the ϵ' dependence as well. The λ values (or effective radiator thicknesses) used are mathematically unique up to a freedom in the ratio of $\lambda_{p'}/\lambda_e$. This feature helps to minimize potential systematic errors in the radiative corrections.

Obviously, a disadvantage of this simple technique is that it neglects the exact angular distributions of radiated events. Thus, improvement on the MERM technique is possible by either determining the exact multiphoton angular distributions of the internal radiation numerically solving Eq. (46), or using the multiphoton peaking approximations described in Sec. IV A, and subsequently folding in these more exact multiphoton angular distributions in an experimental Monte Carlo simulation. However, this is in many cases unwarranted because (i) the only failing of this technique is a slight underestimate of the angular distributions between the particle directions; and (ii) the systematic error in the internal and external radiative effects may be dominated by uncertainties in the theory itself.

Lastly, the MERM technique provides significant gains in computation speed when simulating small experimental acceptances where λ_e, λ_e', and λ_p' are approximately constant and can therefore be evaluated during Monte Carlo initialization. Since the effect of external radiation must be calculated anyway, the effect of internal radiation is included simply by increasing the external radiation bt values by the corresponding λ values. This computational advantage disappears for larger acceptances where the time-consuming determination of the λ's [via evaluation of Eq. (31) and of Eq. II.6 of Ref. [6]] must be performed separately for each event. In such a case one might prefer choosing the λ's according to Eq. (62), and utilize the techniques described in Sec. V A.

VI. DISCUSSION AND SUMMARY

The attractiveness of electron scattering is that the photon couples weakly to the electron and hadrons, simplifying the extraction of information from experimental data. However, in order to extract nuclear structure information or information on the reaction dynamics, one needs to understand the radiative contribution to the measured cross section in detail. In particular, as the momentum transfer increases in electron-induced hadron knockout or hadron production reactions, the internal bremsstrahlung contributions of the hadronic terms cannot be neglected anymore. Up to now the standard for the calculation of radiative effects has been the work of Mo and Tsai [6]. They derived explicit formulas for radiative corrections in an inclusive (e,e') framework, and provided a prescription for unfolding spectra in terms of the energy transfer $\nu=\epsilon-\epsilon'$. It is important to note here that in analyzing results from the $(e,e'p)$ reaction, one must for consistency use form factors derived from previous scattering data using the same radiative correction formulas.

The emphasis of this work is the extension of radiative corrections to coincidence $(e,e'p)$ experiments. Though this work only deals with the $(e,e'p)$ reaction, the formalism presented to apply radiative corrections is general and can easily be adapted for other electron-induced hadron production reactions. For the $(e,e'p)$ reaction one can, in the plane-wave impulse approximation, define a spectral function $S(\mathbf{p}_m,E_m)$ representing the probability of finding a proton in the nucleus with missing energy E_m and momentum $\mathbf{p_m}$. The difference between the calculation presented here and that of Mo and Tsai is that we describe the radiative tails in terms of E_m rather than ω. Specifically, the measured variable E_m is shifted from its value at the scattering vertex by, for elastic ep scattering, exactly the energy of any photon that was emitted during the reaction; it thus provides an ideal coordinate with which to perform radiative computations. Radiation from the scattered proton is taken into account, and constitutes $\geqslant 10\%$ of the internal correction for $Q^2\geqslant 1$ $(\mathrm{GeV}/c)^2$. Also, this contribution varies inversely with the ratio ϵ'/ϵ. The relatively large magnitude of the hadronic contributions to the bremsstrahlung cross sections warrants a detailed investigation of the assumptions and approximations made in the work of Mo and Tsai, in order to successfully apply radiative corrections to electron-induced coincidence reactions.

In order to radiatively correct the full E_m and $|\mathbf{p}_m|$ distribution, one must consider the angular distribution for emitting multiple photons. We have determined that the distribution for emitting a total photon energy ΔE_m is, up to order α^2, equivalent to the emission of any number of soft photons, each with energy less than ΔE_m. Therefore exponentiating δ_{soft} provides a good approximation to the bremsstrahlung cross section for emitting a total photon energy up to a certain cutoff value, the case of practical interest for analyz-

ing experiments. For practical purposes, one employs peaking approximations to estimate radiative effects. This assumes that the emission of photons will take place in the direction of the initial and final electron, with an additional contribution in the direction of the final proton as its energy becomes highly relativistic. At low to intermediate momentum transfers [$Q^2 \approx 1$ $(\mathrm{GeV}/c)^2$ to ≈ 10 $(\mathrm{GeV}/c)^2$], a broad peak will begin to form around the final proton direction. In the full peaking approximation however, the electron-proton interference term is taken to be zero. Thus, if one wants to maintain the correct number of photons emitted but allows an error in the angular distribution due to the peaking approximation, one can assign all the nonpeaked photons to the different peaked directions (''extended'' peaking approximation). One can also add the external bremsstrahlung in a consistent manner to these peaking approximations.

We have compared the radiative correction procedures found in this work with experimental data of the NE18 experiment [11,21,22]. We have used two separate procedures, via Monte Carlo, to simulate the event distributions. In the first procedure we could incorporate in the simulation package either several of the peaking approximations presented or the complete angular distributions for bremsstrahlung. This procedure produced very good agreement with E_m distributions of both the $^1\mathrm{H}(e,e'p)$ and $^2\mathrm{H}(e,e'p)$ reactions, at momentum transfers between 1 and 7 $(\mathrm{GeV}/c)^2$. It was also used to simulate a detailed angular distribution of the $^1\mathrm{H}(e,e'p)$ events for photon energies above 20 MeV, and excellent agreement was found. The second procedure hinges on the peaking approximations and extends the usual equivalent radiator method to reproduce both the event distribution of the $^1\mathrm{H}(e,e')$ reaction in terms of the scattered electron energy and the $^1\mathrm{H}(e,e'p)$ reaction in terms of missing energy. These constrain the choice of three equivalent radiators of different thickness (for the incoming and outgoing electron and the proton). It is shown that this simple procedure describes the $^1\mathrm{H}(e,e'p)$ tail distribution in terms of E_m very well. Since the method hinges on the (angle) peaking approximation, we also show from the NE18 $^1\mathrm{H}(e,e'p)$ data why this assumption works well. Unless one is interested in a detailed and high-precision understanding of angular distributions of $(e,e'p)$ reaction, the ''modified'' equivalent radiator method provides a simple, effective procedure for radiative corrections.

ACKNOWLEDGMENTS

This work was supported in part by the U.S. Department of Energy under Contract No. DE-AC02-76ER03069 (MIT) and by the U.S. National Science Foundation under Grant No. PHY-9115574 (Caltech). R.G.M. acknowledges the support from the NSF. B.W.F. acknowledges the support of the Sloan Foundation.

APPENDIX: EVALUATION OF BREMSSTRAHLUNG INTEGRALS

This appendix evaluates the integrals necessary for the evaluation of $B(p_i,p_j,\Delta E)$ as given by Eq. (32). The two cases $i=j$ and $i\neq j$ are considered separately.

First consider the case $i=j$ which requires the evaluation of $\overline{B}(p,p,\Delta E)$. In this case $p_x^2=p^2$ and the integrands in Eq. (32) are independent of x, yielding

$$\overline{B}(p,p,\Delta E) = 4\pi\left[\ln\left(\frac{\Delta E}{p^0}\right)+\frac{p^0-|\mathbf{p}|}{2|\mathbf{p}|}\ln\left(\frac{p^0-|\mathbf{p}|}{p^0+|\mathbf{p}|}\right)+\ln\left(\frac{2p^0}{p^0+|\mathbf{p}|}\right)\right]. \tag{A1}$$

For the case $i\neq j$, consider the ΔE dependent part of $B(p_i,p_j,\Delta E)$ [note that the other two terms go to zero in the relativistic limit ($|\mathbf{p}|\to\infty$)],

$$\int_0^1 \frac{dx}{p_x^2}\ln\left[\frac{\Delta E}{p_j^0+x(p_i^0-p_j^0)}\right]. \tag{A2}$$

The evaluation of this integral in terms of Spence functions is standard. Writing

$$p_x^2=\alpha(x-x_+)(x-x_-), \tag{A3}$$

where

$$\alpha=(p_i-p_j)^2 \tag{A4}$$

and

$$x_\pm=\frac{2p_j^2-2p_i\cdot p_j\pm\sqrt{4(p_i\cdot p_j)^2-4p_j^2(p_i-p_j)^2}}{2\alpha} \tag{A5}$$

implies

$$\begin{aligned}\int_0^1 \frac{dx}{p_x^2}\ln\left[\frac{\Delta E}{p_j^0+x(p_i^0-p_j^0)}\right] &= \frac{1}{\alpha(x_--x_+)}\left[\ln\left(\frac{p_j^0+x_+(p_i^0-p_j^0)}{\Delta E}\right)\ln\left(\frac{x_+-1}{x_+}\right)-\ln\left(\frac{p_j^0+x_-(p_i^0-p_j^0)}{\Delta E}\right)\ln\left(\frac{x_--1}{x_-}\right)\right.\\ &\left.-\Phi\left(\frac{(p_i^0-p_j^0)(x_+-1)}{p_j^0+x_+(p_i^0-p_j^0)}\right)+\Phi\left(\frac{(p_i^0-p_j^0)x_+}{p_j^0+x_+(p_i^0-p_j^0)}\right)+\Phi\left(\frac{(p_i^0-p_j^0)(x_--1)}{p_j^0+x_-(p_i^0-p_j^0)}\right)-\Phi\left(\frac{(p_i^0-p_j^0)x_-}{p_j^0+x_-(p_i^0-p_j^0)}\right)\right].\end{aligned} \tag{A6}$$

Here the usual identity

$$\int_0^1 \frac{\log(b-cx)}{x-a} = \log(b+ac)\log\left(\frac{a-1}{a}\right) - \Phi\left(\frac{-c(1-a)}{b+ac}\right) + \Phi\left(\frac{ac}{b+ac}\right) \tag{A7}$$

has been used.

[1] H.A. Bethe and W. Heitler, Proc. R. Soc. London, Ser. A **146**, 83 (1934).
[2] J. Schwinger, Phys. Rev. **76**, 790 (1949).
[3] D.R. Yennie, S. Frautschi, and H. Suura, Ann. Phys. (N.Y.) **13**, 379 (1961).
[4] Y.S. Tsai, Phys. Rev. **122**, 1898 (1961).
[5] N.T. Meister and D.R. Yennie, Phys. Rev. **130**, 1210 (1963).
[6] L.M. Mo and Y.S. Tsai, Rev. Mod. Phys. **41**, 205 (1969).
[7] C. de Calan, H. Navelet, and J. Picard, Nucl. Phys. **B348**, 47 (1991).
[8] J.A. Templon, C.E. Vellidis, R.E.J. Florizone, and A.J. Sarty, Phys. Rev. C **61**, 014607 (2000).
[9] Y.S. Tsai, Rev. Mod. Phys. **46**, 815 (1974).
[10] J. Friedrich, Nucl. Instrum. Methods **129**, 505 (1975).
[11] N.C.R. Makins *et al.*, Phys. Rev. Lett. **72**, 1986 (1994); T.G. O'Neill *et al.*, Phys. Lett. B **351**, 87 (1995).
[12] T. de Forest, Jr., Nucl. Phys. **A132**, 305 (1969).
[13] P.E. Bosted *et al.*, Phys. Rev. Lett. **68**, 3841 (1992).
[14] A. Lung *et al.*, Phys. Rev. Lett. **70**, 718 (1993).
[15] R.C.D. Walker, Ph.D. thesis, California Institute of Technology, 1989.
[16] R.A. Early, Nucl. Instrum. Methods **109**, 93 (1973).
[17] N.C.R. Makins, Ph.D. thesis, Massachusetts Institute of Technology, 1994.
[18] T.G. O'Neill, Ph.D. thesis, California Institute of Technology, 1994.
[19] M. Gari and W. Krümpelmann, Z. Phys. A **322**, 689 (1985).
[20] K. Holinde and R. Machleidt, Nucl. Phys. **A256**, 479 (1976).
[21] H.J. Bulten *et al.*, Phys. Rev. Lett. **74**, 4775 (1995).
[22] J.F.J. van den Brand *et al.*, Phys. Rev. D **52**, 4868 (1995).
[23] L.I. Schiff, Phys. Rev. **87**, 750 (1952).
[24] E. Borie and D. Drechsel, Nucl. Phys. **A167**, 369 (1971).